SANDIA REPORT

SAND2008-6014~~119632~~XXXXX
Unlimited Release
Printed September 2008

IMPROVED NUMERICAL METHODS FOR MODELING RIVER-AQUIFER INTERACTION

Suzanne Tillery, James Phillip King, Vince Tidwell

Prepared by
Sandia National Laboratories
Albuquerque, New Mexico 87185 and Livermore, California 94550

Sandia is a multiprogram laboratory operated by Sandia Corporation,
a Lockheed Martin Company, for the United States Department of Energy's
National Nuclear Security Administration under Contract DE-AC04-94AL85000.

Issued by Sandia National Laboratories, operated for the United States Department of Energy by Sandia Corporation.

Available to DOE and DOE contractors from

U.S. Department of Energy
Office of Scientific and Technical Information
P.O. Box 62
Oak Ridge, TN 37831

Telephone: (865) 576-8401
Facsimile: (865) 576-5728
E-Mail: reports@adonis.osti.gov
Online ordering: http://www.osti.gov/bridge

Available to the public from

U.S. Department of Commerce
National Technisa Information Service
5285 Port Royal Rd.
Springfield, VA 22161

Telephone: (800) 553-6847
Facsimile: (703) 605-6900
E-Mail: orders@ntis.fedworld.gov
Online order: http://www.ntis.gov/help/ordermethods.asp?loc=7-4-0#online

SAND2008-6014~~119632~~XXXXX
Unlimited Release
Printed September 2008

IMPROVED NUMERICAL METHODS FOR MODELING RIVER-AQUIFER INTERACTION

Suzanne Tillery, James Phillip King
New Mexico State University
Department of Civil and Geological Engineering
P.O. Box 30001, MSC-3CE
Hernandez Hall
Las Cruces, NM 88003-8001

Vincent Tidwell
Geohydrology Department 6313
Sandia National Laboratories
P.O. Box 5800
Albuquerque, NM 87185-0735

ABSTRACT

A new option for Local Time-Stepping (LTS) was developed to use in conjunction with the multiple-refined-area grid capability of the U.S. Geological Survey's (USGS) groundwater modeling program, MODFLOW-LGR (MF-LGR). The LTS option allows each local, refined-area grid to simulate multiple stress periods within each stress period of a coarser, regional grid. This option is an alternative to the current method of MF-LGR whereby the refined grids are required to have the same stress period and time-step structure as the coarse grid. The MF-LGR method for simulating multiple-refined grids essentially defines each grid as a complete model, then for each coarse grid time-step, iteratively runs each model until the head and flux changes at the interfacing boundaries of the models are less than some specified tolerances.

Use of the LTS option is illustrated in two hypothetical test cases consisting of a dual well pumping system and a hydraulically connected stream-aquifer system, and one field application. Each of the hypothetical test cases was simulated with multiple scenarios including an LTS scenario, which combined a monthly stress period for a coarse grid model with a daily stress period for a refined grid model. The other scenarios simulated various combinations of grid spacing and temporal refinement using standard MODFLOW model constructs. The field application simulated an irrigated corridor along the Lower Rio Grande River in New Mexico, with refinement of a small agricultural area in the irrigated corridor.

The results from the LTS scenarios for the hypothetical test cases closely replicated the results from the true scenarios in the refined areas of interest. The head errors of the LTS scenarios were much smaller than from the other scenarios in relation to the true solution, and the run times for the LTS models were three to six times faster than the true models for the dual well and stream-aquifer test cases, respectively. The results of the field application show that better estimates of daily stream leakage can be made with the LTS simulation, thereby improving the efficiency of daily operations for an agricultural irrigation system.

ACKNOWLEDGEMENTS

The authors appreciatively acknowledge support for Sue Tillery provided by Sandia National Laboratories' through a Campus Executive Laboratory Directed Research and Development (LDRD) research project.

~~Funding for this study was provided by <???. S. Tillery is funded by Sandia National Laboratories' through an Excellence in Engineering Fellowship Laboratory> Directed Research and Development (LDRD) research project.~~

TABLE OF CONTENTS

TABLE OF FIGURES

TABLE OF TABLES

1. PROJECT DESCRIPTION AND BACKGROUND

1.1 Background

This project addresses a fundamental shortcoming in traditional modeling projects, which is that groundwater and surface water are modeled in essentially different spatial, dimensional, and temporal domains, requiring modelers to focus on either surface or groundwater, with an oversimplified representation of the other. This research focuses on modeling the interaction between surface water and groundwater and its implications for resource management.

Regional groundwater models tend to be three dimensional, finite element/finite difference models with cell sizes on the order of a kilometer. The temporal resolution is often limited to seasonal or even annual time frames, making support for within-season management decisions difficult. Surface water models tend to represent the river as nodes which simulate diversions, inflow points and so on. These nodes are connected by links that roughly simulate the hydrologic behavior of the river between the nodes. Time-steps may be days, hours, or even minutes for flow routing calculations.

The discrepancies between the conceptual representation of surface and groundwater models can be overcome with integrated surface water – groundwater modeling, but the data needs and computational requirements are far greater than for a single domain model. However, with the rise of advanced code development and geometrically increasing computing power, such model development on a regional scale is now becoming feasible.

1.2 Justification

When a surface water flow system is closely related to the underlying groundwater flow system, both systems are equally important and need to be simulated in an integrated model that's conceptualized and constructed to simulate surface water flow movement, groundwater flow movement and the interactions between them at the same time. For example, a stream flow/groundwater flow model would best be calibrated by using stream stages and flows, as well as groundwater levels. However, if the grid spacing throughout the domain is defined to be relatively small to meet the accuracy needs in the regions of strong stream-aquifer interaction, there are many inefficient and redundant calculations being performed in the regions away from the area of strong interaction. It is therefore desirable to use an embedded mesh, or local grid refinement, to cluster grid points in regions where they are most needed, such as regions where the solution has steep gradients, while allowing coarser grid resolution in regions with little variation over larger distances. Adding refinement in space over rectangular patches will give the most accurate and efficient solution method for solutions of surface water flow systems and groundwater flow systems that have strong hydraulic connectivity.

There are several refinement methods that may be applied: (1) globally refined grids where the grid is refined over the entire domain, which may be computationally intensive and require extensive labor resources to develop data sets defining the entire domain when only a local area

is of interest, (2) variably spaced grids where a fine grid is defined locally with moderate increases in computational time, but still results in refinement in areas that do not need it as the same grid spacing extends out to boundaries, and (3) locally refined grids which link two or more different-sized finite-difference grids: a coarse parent grid covering a large area including regional boundary conditions, and a fine child grid covering only the area of interest. Local grid refinement can be vertical as well as horizontal, and the grids can be linked by two-way communication between the grids, so that feedback from the child grid to the parent grid is included.

Quite often, the surface water and groundwater equations for a coupled system are solved at the same time-step. However, in the vicinity of a strong stream-aquifer interaction, a small time-step is required to simulate the interactions properly, while at distance in the aquifer, a much larger time-step may be adequate to accurately simulate the groundwater flow. Therefore, instead of using a common, global time-step for both flow regimes, a local time-stepping procedure can be used such that the regions requiring a small time-step can be simulated at a small time-step, while other regions can be simulated at a larger time-step. Adding local time-stepping to a locally refined grid model will maintain the solution accuracy while reducing the run time of the simulation.

Based on literature including Berger and Leveque 1998; Chang et al. 2005; Crossley and Wright 2005; Crossley 1999; Crossley et al. 2003; Hu et al. 2006; Imamura et al. 2005; Kirby 2002; Lackey and Sotiropoulos 2005; Lamby et al. 2005; Niessner and Helmig 2006; Panday and Huyakorn 2004; Perotto 2006; Qian 2006; Tang and Warnecke 2006; and Zhang et al. 1994, the consensus is clear that it is more efficient and accurate for a surface water/groundwater system with strong hydraulic connectivity to simulate these areas with a refined grid child model running at a smaller time-step than the coarse grid parent model.

1.3 Objective

The purpose of this research was to modify the MODFLOW-LGR (MF-LGR) software to allow local time-stepping (LTS) for the child models, while simulating the parent model at the global time-interval. This would allow the child model simulation time-intervals to be smaller than the parent model time-intervals, in order to capture transient events in areas with strong hydraulic connectivity between the surface water and the groundwater, while leaving the coarser grid parent model at a larger time-interval that is appropriate in regions of little, or minimal, hydraulic connectivity. The goal was to derive as much detailed, relevant information from a model as possible, without imposing an excessive computational burden on the system. It is generally accepted that the *de facto* industry standard for groundwater modeling software is the MODFLOW series of software developed by the United States Geological Survey (USGS). Recent additions to this software supporting multiple-refined-grid areas (i.e. MF-LGR) make it an ideal base for implementing a local time-stepping option. MF-LGR Version 1.1 has the capability to simulate multiple, fine-scale embedded child grids within a coarse parent grid; however, all the grids must run at the same global time-interval of the parent grid.

1.4 Approach

The USGS MODFLOW series of groundwater modeling software may be used as an integrated model, as it provides the ability to simulate stream and other surface water flow along with simulating groundwater flow. Mehl and Hill (2005) developed a Local Grid Refinement (LGR) package to allow users of MODFLOW-2005 (Harbaugh 2005) to create simulations that use a single locally refined grid, denoted as a child model, that is embedded within a coarser grid, that is denoted as the parent model. Mehl and Hill (2007) subsequently enhanced the LGR package to simulate multiple, locally refined grids within the coarse grid, resulting in a version of MODFLOW-2005 designated as MODFLOW-LGR (MF-LGR), Version 1.1, dated 08/8/2007. This implementation iteratively couples one parent model and one or more child models such that the heads and fluxes are balanced across the shared interfacing boundaries.

Flow calculations in the MODFLOW software uses the conventional approach of global time-stepping, where the solution is advanced in time through a series of updates in which all cells are integrated to the same point in time. However, when developing an integrated coupling for stream flow and groundwater flow in a strongly-interactive stream-aquifer system, the time-steps in the vicinity of the stream become the global time-step for the entire domain even though the solution accuracy of the aquifer away from the stream can be met with larger time-steps. Using a small time-step throughout the domain results in an excessive and redundant computational burden. A solution to this problem is to use local time-stepping such that the refined areas that change quickly with time are simulated at a smaller time-step, while the coarser regions that change slowly are only evaluated at a larger time-step, with the goal of reducing run times while maintaining solution accuracy.

1.5 Methodology

The main factor in implementing local time-stepping for the MF-LGR software is describing how the child grid stress periods and time-steps relate to the parent grid stress periods and time-steps. Within MODFLOW, a stress period is defined as the time interval associated with changing conditions or ‘stresses’ on the system. For example, specified pumping rates or specified stream stages may only change on stress period intervals. Transient simulations in MODFLOW are based on allowing the user to specify a number of stress periods, a time length for each stress period, a number of time-steps within each stress period, and a geometric multiplication factor for the time-steps (Harbaugh 2005). For example, the time-steps for a simulation with three stress periods are shown in Figure 1. The first stress period has four time-steps, evenly spaced; the second stress period has five time-steps geometrically increasing by a factor of 1.3; and the third stress period has six time-steps geometrically decreasing by a factor of 0.65.

The approach used by this research to implement local time-stepping in a simulation with one parent grid and one or more child grids is to require that the length and number of the child grid stress periods must match exactly the length and number of the parent grid time-steps. Then within each child grid stress period, one time-step and a multiplier of one must be specified.

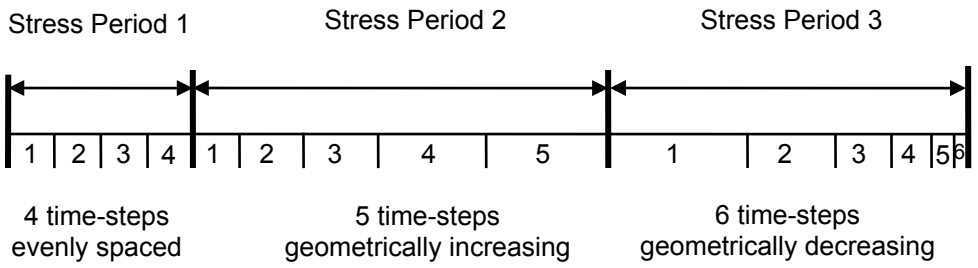

Figure 1. MODFLOW stress periods and time-steps

Using the above example with three parent stress periods, the first parent stress period is expanded, as shown in Figure 2, with the corresponding child stress periods and time-steps. This figure shows that each time-step in the parent stress period is the same length as the corresponding stress period in the child grid, and that within each child stress period there is one time-step. The same relationships must be retained for the second and third parent stress periods in this example, with the result of 15-child stress periods at the same time lengths and in the same order as the 15 time-steps of the parent model.

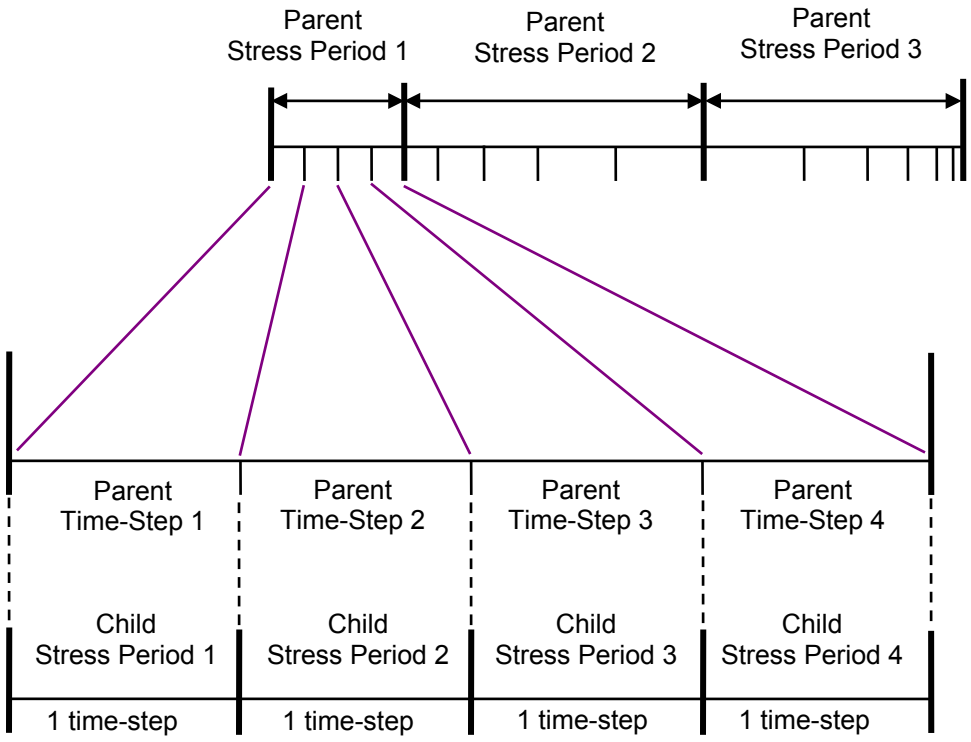

Figure 2. Parent and child stress periods and time-steps

1.6 Conceptual Model

A conceptual model is described for the processing that occurs within each parent model stress period. This conceptual model shows how the child model stress- periods and time-steps are related to the parent model stress periods and time-steps. Figure 3 gives a schematic for this conceptual model, with narrative information provided for the loops and the numbered blocks in the schematic. The shaded blocks in the conceptual model indicate the locations where changes to the software were required to implement the local time-stepping option.

Parent grid stress period loop: This loop is used to advance the model through each of the parent grid stress periods.

Parent grid time-step loop / Child grid stress period & time-step loop: This loop is used to advance the model through each of the parent grid time-steps. For the LTS option, each parent grid time-step corresponds to the single time-step of a child grid stress period.

Child grid loop: This grid loop is used to setup the stress period and time-step for each child grid corresponding to each parent grid time-step.

Block 1. Setup child grid stress period and advance child grid time-step: For each parent grid time-step, the setup files for each child grid are read for the current child stress period. Then the child grid is advanced to the time-step of the new stress period, which includes saving the current head values as the previous head values.

LGR iteration loop: The LGR iteration loop repeats in each parent model time-step and solves for each of the grids in the simulation until the changes in head and flux across the interfacing boundaries of the parent and child grids are less than user specified tolerances.

Grid loop (1): The grid loop in the LGR iteration loop is used to arrive at a solution to the finite difference equations for each grid in the simulation.

Finite difference solution iteration loop: The finite difference solution iteration loop creates the finite difference equations and applies the user specified solver method to them. This loop iterates until either the maximum number of iterations is reached, or the change in head between iterations is less than a user specified tolerance.

Grid loop (2): The second grid loop is invoked after the LGR solution for this parent time- step has converged. This loop is used to calculate and/or output the volumetric budget information when requested.

Block 2. If child grid, use stress period and time-step from child: If this is a child grid, then extract the stress period and time-step numbers from the child grid to include in the output file.

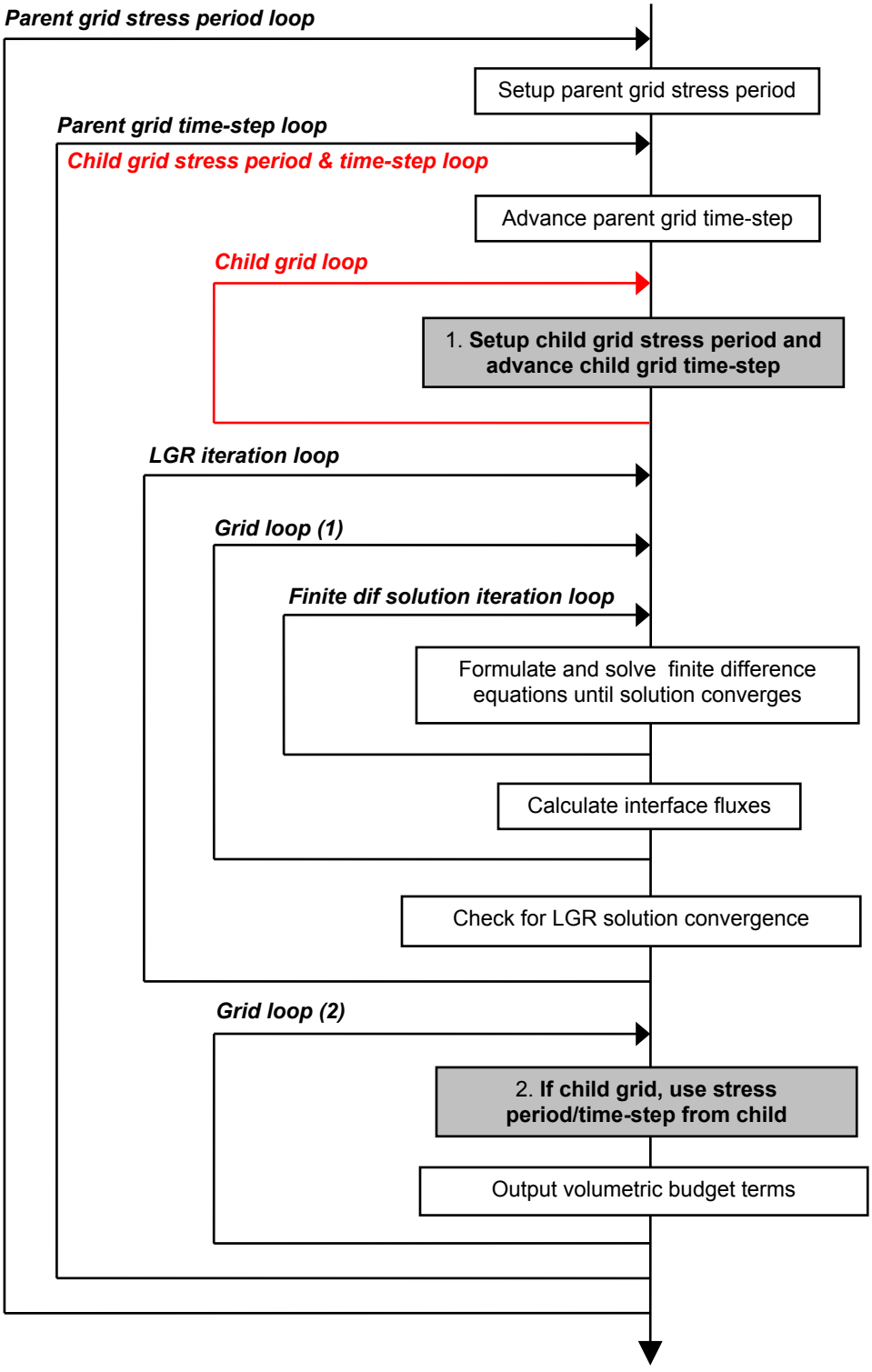

Figure 3. Conceptual model for parent model stress periods

2. TEST CASES

2.1 Introduction

Three test cases were used to evaluate the addition of the Local Time Stepping (LTS) option to the MODFLOW-LGR (MG-LGR) software. The first test case is based on a hypothetical steady-state example described by Mehl and Hill (2007) that simulates drawdown from two identical wells. The second test case is based on a hypothetical steady-state example used by Mehl and Hill (2005) that simulates stream-aquifer interactions. The third test case is for a field application of an irrigated area in the Rincon Valley, New Mexico, based on a regional MODFLOW model developed by Weeden and Maddock (1999).

2.2 Dual Well Test Case

The multiple-refined area example of Mehl and Hill (2007) describes a simulation for two areas of pumping within an aquifer. Figure 4 shows a graphic of the dual well system, with the wells screened in a three-foot thick, confined aquifer layer. Q_1 represents the pumping rate from Well 1, and Q_2 represents the pumping rate from Well 2. The confined aquifer is isotropic and homogeneous, with a hydraulic conductivity of 5.0×10^{-4} m/s, and a specific storage value of 1.0e-04 m^{-1}.

2.2.1 Model Parameters

The model domain is 999 m in the x-direction and 450 m in the y-direction, with the origin for these directions at the lower left-hand corner of the domain, from a plan view. There are constant head, h_t, boundaries for all times of 10 m on the left boundary and on the right boundary. The boundaries located at y = 450 m for all x-locations, and y = 0 m for all x-locations are specified as no-flow boundaries. Initial heads, h_o, throughout the model area are specified as 10 m. Well 1 is located at x = 272.88 m, y = 220.5 m, and Well 2 is located at x = 726.12 m, y = 220.5 m.

2.2.2 Model Grid Discretization

Three sets of grid discretizations were used for this test case, a globally fine grid, a globally coarse grid which is also used for the parent grid, and the refined grids in the child areas of the model domain.

Globally Fine Grid: The globally fine grid model has 450 rows at a height of 1 m each, and 972 columns at a width of 1.028 m each, for a total row length of 450 m and a total column width of 999 m. There is one 3 m thick confined layer in this grid and the two wells for this resolution are located at row 230, column 266 and at row 230, column 707. The relative position of the first refined child grid within this grid can be specified as a rectangle with corners at row 176, column 194 and at row 275, column 347. In terms of x and y, this rectangle has corners at

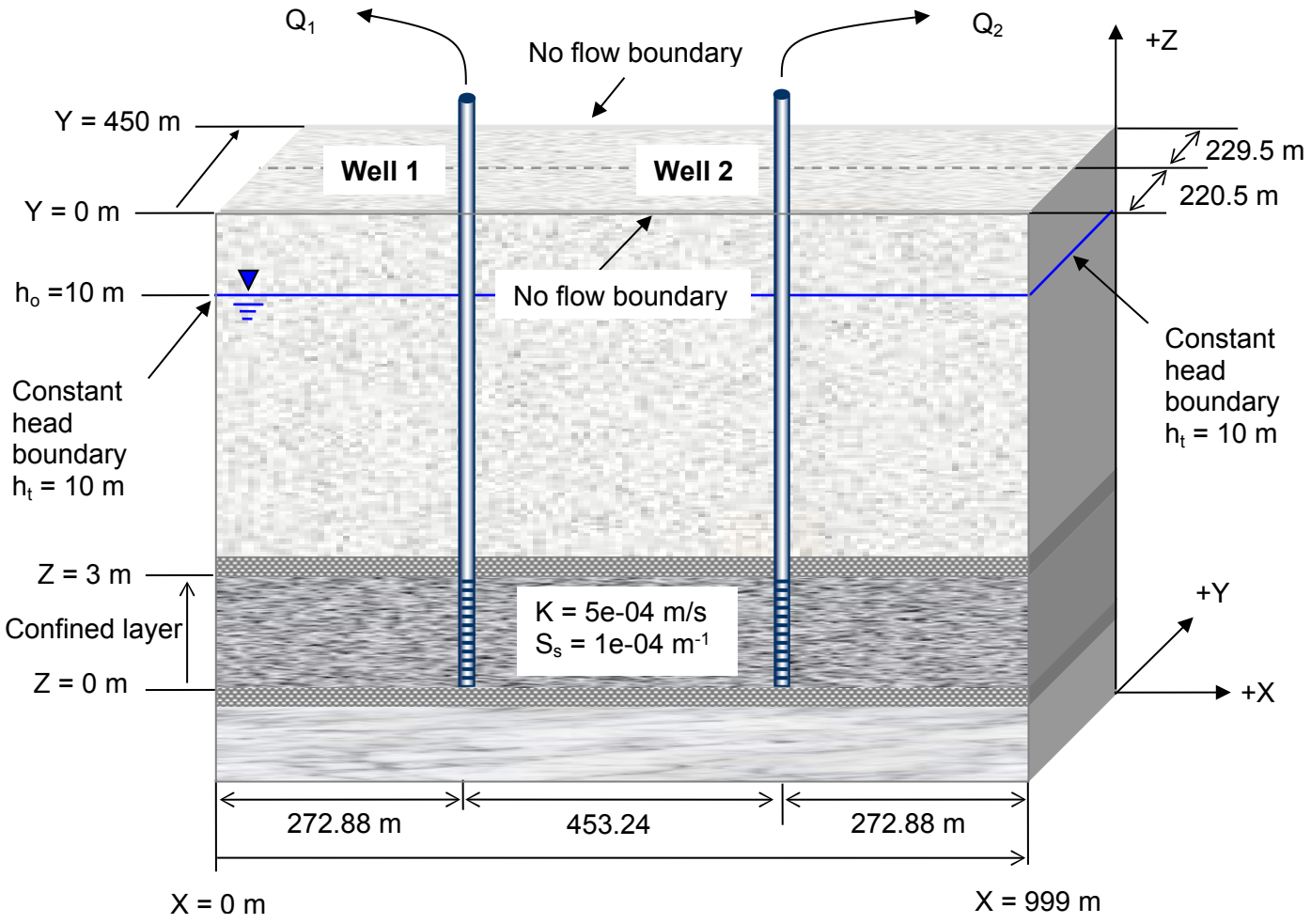

Figure 4. Dual well system

x = 198.88 m, y = 175.5 m and at x = 356.13 m, y = 274.5 m. The relative position of the second refined child grid within this grid can also be specified as a rectangle with corners at row 176, column 626 and at row 275, column 779. This corresponds to x and y corner locations of x = 642.88 m, y = 175.5 m and at x = 800.13 m, y = 274.5 m.

Globally Coarse and Parent Grids: The second grid resolution is for the globally coarse grid model and for the coarse parent grid of the LTS model. The coarse grid has 50 rows at a length of 9 m each, and 108 columns at a width of 9.25 m each, for the same total row length of 450 m and total column width of 999 m as the globally fine grid. This grid has one 3 m thick confined layer, and the two wells are located at row 26, column 30 and at row 26, column 79. The first refined child grid is located within the rectangle defined by corners at row 20, column 22, and at row 31, column 39. The second refined child grid is located within the rectangle specified by corners at row 20, column 70, and at row 31, column 87. The relative x and y locations of the wells and the child refined areas are the same for the coarse grid as for the globally fine grid.

Refined Child Grid: The third grid resolution is for the two refined, child grids around the wells. The child grids are each a 9:1 ratio refinement of the coarse parent grid and have 100 rows at a length of 1 m each and 154 columns at a width of 1.028 m each, for a total row length of 100 m and a total column width of 158.28 m. There is a single layer for this grid resolution, indicating there is no vertical refinement for this test case. The well in the first child grid refinement is located at row 55, column 73, or at x = 74.51 m, y = 54.5 m. The second well is located at row 55, column 82, or at x = 83.76.m, y = 54.5 m in the second child grid refinement.

2.2.3 Model Time Resolutions

The example model for the dual well system by Mehl and Hill (2007) was a steady-state simulation. To test the local time-stepping implementation, the steady-state globally fine grid example was converted to a transient simulation with pumping at daily stress-periods for 360 days, which will represent the true solution both spatially and temporally. To create the daily stress-periods, arbitrary monthly (assuming 30-day months) pumping rate values were arrived at assuming a seasonal flow pattern with little or no pumping in the winter and highest pumping in the summer. Then each monthly volume pumped was randomly divided into 30 daily values, with the total daily volume pumped equal to the monthly volume pumped, but no linear pattern to the daily values within the month. The daily and monthly pumping rates are shown graphically in Figure 5.

The three sets of grid resolutions were simulated with various combinations of daily and monthly stress periods and time-steps, with the stress periods corresponding to the pumping intervals. Table 1 shows the combinations of grid resolutions, stress periods and time-steps that were simulated.

2.2.4 Model Error Analysis

Error analysis for this case study was made by comparing results of the globally fine daily model, which is considered to be the true results, with the results from the other simulations

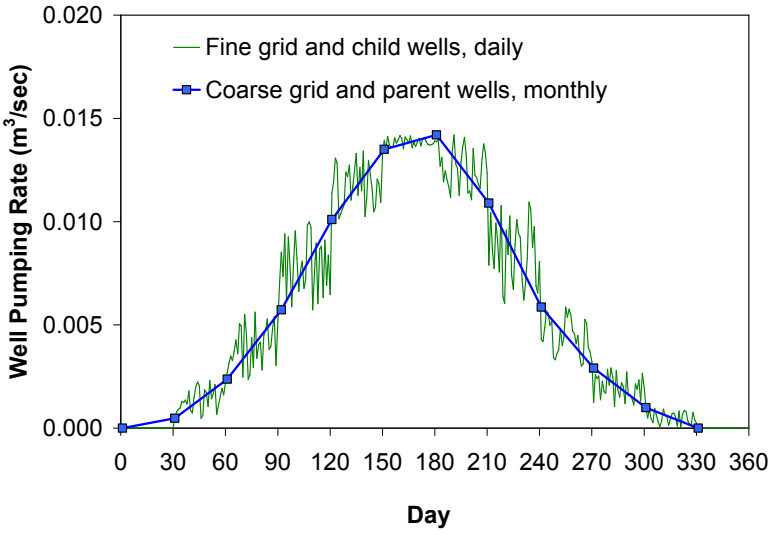

Figure 5. Dual well system pumping rates

Table 1. Dual well grid resolutions, stress periods and time-steps

Grid Resolution	Stress Period Length	Number of Time-Steps per Stress Period
Globally Fine	1 Day	1
Globally Fine	1 Month	30
Globally Coarse	1 Day	1
Globally Coarse	1 Month	30
Coarse Parent with Fine Child	Parent: 1 Month Child: 1 Day	30 1

identified in Table 1. Several metrics were used to evaluate the relative accuracies of the various simulations compared to the true results, including the differences in head at Well 1, the maximum head differences in the parent and child areas, and the Root-Mean-Squared-Error (RMSE) of the head differences in the parent and child areas. These values were calculated for each stress period, with the RMSE calculated as:

$$E_R = \frac{1}{nobs}\sqrt{\sum \left(h_{obs} - h_{sim}\right)^2} \tag{1}$$

where E_R is the RMSE of the head differences; *nobs* is the number of observations; h_{obs} is the observed, or true, head value; and h_{sim} is the simulated head value.

Errors were only calculated for the left half of the domain, including one refined area, due to the symmetry of the test case. There were 293 observation nodes designated in what is referred to as

the parent area of the domain. These nodes coincide with coarse grid cells, and were specified starting at row 2, column 2, and then located subsequently every 3 rows and every 3 columns, excluding the area of the refined grid. Another 215 observation nodes were specified in the refined child area of the domain, including the boundary nodes between the parent and child grid, but excluding the grid cell containing the well. This provides observations in the child refined area at every child grid node corresponding to a coarse or parent grid node. The child observation nodes were specified starting at row 1, column 1, and then located subsequently every 9 rows and every 9 columns.

2.3 Stream-Aquifer Test Case

Example 3 of Mehl and Hill (2005) describes a simulation for a three-dimensional steady state, homogeneous model domain with a stream hydraulically connected to an unconfined aquifer. Figure 6 gives a plan view of this stream aquifer system with the area of local refinement delineated within the plan view and Figure 7 shows a graphic of this stream-aquifer system.

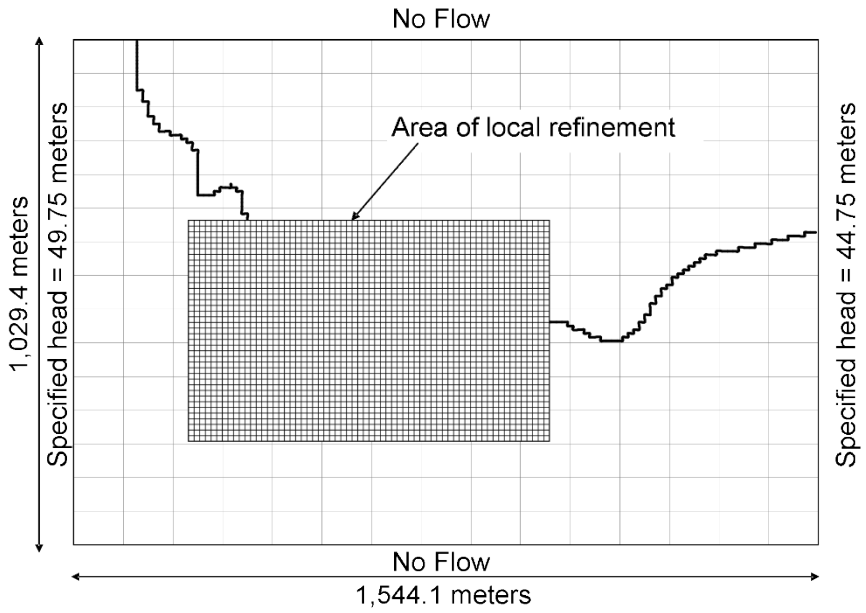

Figure 6. Plan view of stream-aquifer system (adapted from Mehl and Hill 2005)

The model domain is divided into 9 layers with the layers tilted from left (at x = 0 m) to right (at x = 1544.1 m), with the left end of each layer 5 meters higher than the corresponding right end of the layer. The top layer is designated as an unconfined aquifer, and the remaining layers are designated as confined/unconfined aquifers. The layers are homogeneous and horizontally isotropic, with a horizontal hydraulic conductivity of 1.0e-04 m/s, a vertical anisotropy ratio of 0.9, a specific yield value for the unconfined layers of 0.25, and a specific storage value for the confined layers of 1.0e-04 m^{-1}.

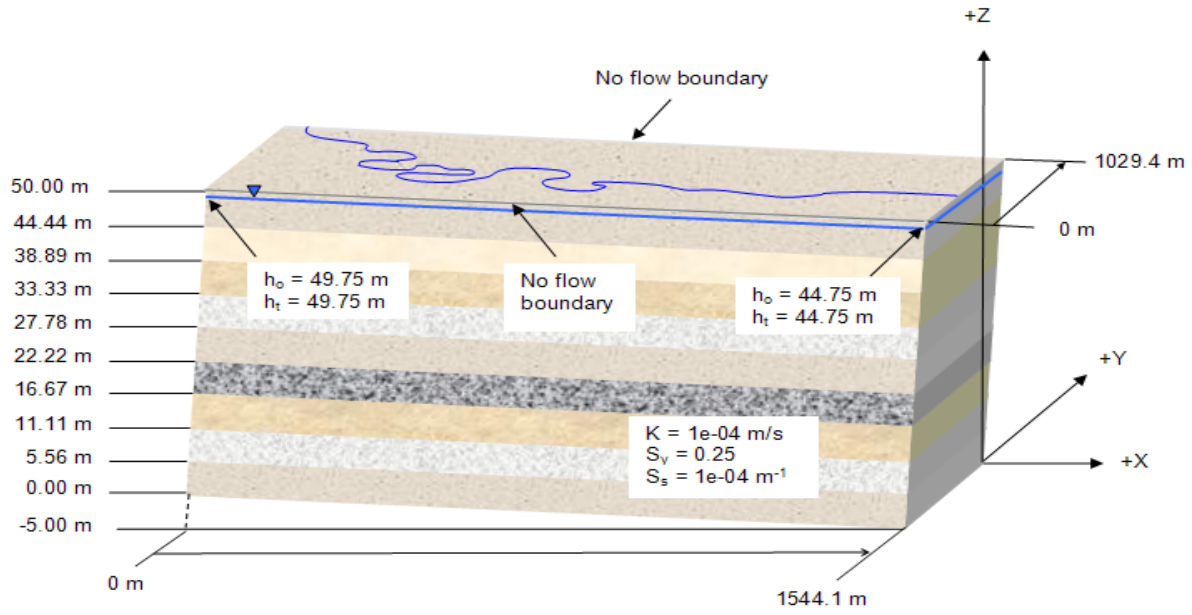

Figure 7. Stream-aquifer system

2.3.1 Model Parameters

The stream has a total length of 3,409 m, with the inlet stage at 50 m and the outlet stage at 45 m, with a resulting gradient along the river of 0.00147. The width of the river is constant at 1 m, with a streambed thickness of 0.5 m and a streambed conductivity of 1 m/day. The land surface elevation is 50 m at the left boundary of the model domain, and drops linearly to 45 m at the right boundary. The thickness of the model is uniform at 50 m, resulting in a linear gradient at the bottom boundary.

The model domain is 1544.1 m in the x-direction, 1029.4 m in the y-direction, and 50 m in the z-direction, with the origin for these directions at the lower left-hand corner of the domain from a plan view. There are constant head, h_t, boundaries for all times of 49.75 m on the left boundary and 44.75 m on the right boundary. The boundaries for all times for all layers located at y = 1029.4 m for all x-locations, and y = 0 m for all x-locations are specified as no-flow boundaries. Initial heads, h_o, for all layers are sloped linearly from left to right, with 49.75 m at the left edge of each layer, and 44.75 m at the right edge of each layer.

2.3.2 Model Grid Discretization

Three sets of grid discretizations were used for this test case, a globally fine grid, a globally coarse grid which is also used for the parent grid, and the refined grid in the child area of the model domain.

Globally Fine Grid: The globally fine grid model has 135 rows at a length of 7.625 m each, and 135 columns at a width of 11.4378 m each, for a total row length of 1029.4 m and a total column width of 1544.1 m. There are nine 5.56 m thick layers in this grid, with the column 1

edge 5 m higher than the column 135 edge of each layer. The relative position of the refined child grid within this grid can be specified as a rectangle with corners at row 50, column 14 and at row 104, column 77. In terms of x and y, this rectangle has corners at x = 154.41 m, y = 377.45 m and at x = 874.99 m, y = 789.21 m.

Globally Coarse and Parent Grids: The second grid resolution is for the globally coarse grid model and for the coarse parent grid of the refined child grid model. The coarse grid has 15 rows at a length of 68.627 m each, and 15 columns at a width of 102.94 m each, for the same total row length of 1029.4 m and total column width of 1544.1 m as the globally fine grid. The rows and columns of this grid are nine times larger than the globally fine grid. There are three 16.67 m thick layers at this resolution, with each layer composed of three of the globally fine grid layers. The refined child grid is located within the rectangle defined by corners at row 6, column 2, and at row 12, column 9.

Refined Child Grid: The third grid resolution is for the refined, child grid around the meanders of the stream. The child grid is a 3:1 ratio refinement of the coarse parent grid, and has 19 rows at a length of 22.856 m each, 22 columns at a width of 34.313 m each, for a total row length of 411.76 m and a total column width of 720.58 m. The rows and columns of this grid are three times larger than the globally fine grid. There are five layers for this grid resolution, corresponding to the top five layers of the globally fine grid.

2.3.3 Model Time Resolutions

The example model for the stream-aquifer system by Mehl and Hill (2007) was a steady-state simulation. To test the local time-stepping implementation, the steady-state globally fine grid example was converted to a transient simulation with specified stream stages at daily stress periods for 360 days, which will represent the true solution both spatially and temporally. Figure 8 shows the locations of the river cells for each grid resolution, which are the points where the stream stages are applied to the model.

To create the daily stress periods, arbitrary small increments of stage were added or subtracted to the original steady-state stages for each day. The monthly stress period stages were then extracted from the daily stages at 30-day intervals. Figure 9 shows the daily and monthly stream stages for each grid resolution. For the globally fine grid, the stream stages shown are for the river cell located at the inlet of the river to the model domain; for the monthly parent and daily child grids, the stream stages shown are for the river cells located at the boundary of the coarse parent and refined child models, and represent the stage at the inlet to the refined area.

The three sets of grid resolutions were simulated with various combinations of daily and monthly stress periods and time-steps, with the stress periods corresponding to the changes in stage at the river cells. Table 2 shows the combinations of grid resolutions, stress periods and time-steps that were simulated.

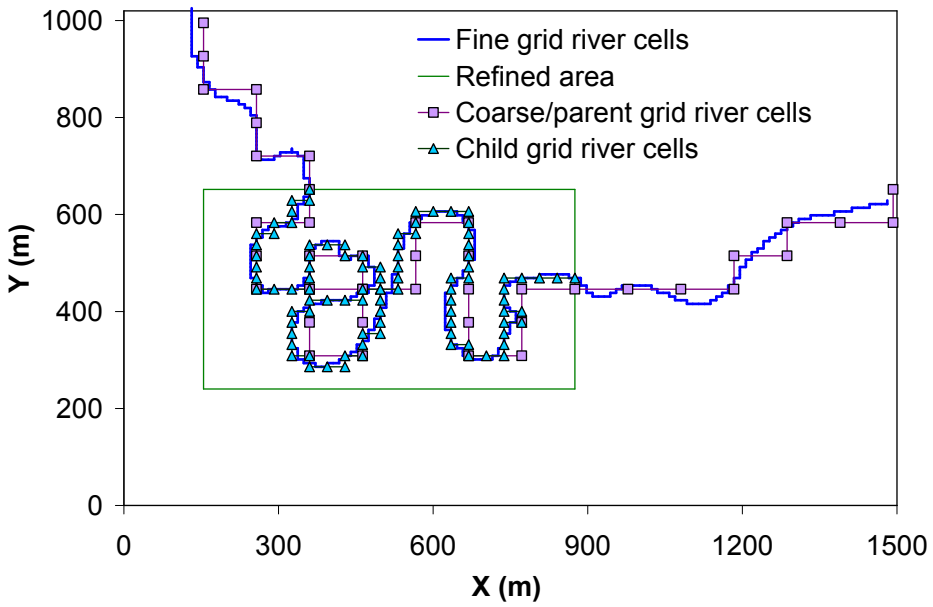

Figure 8. Stream-aquifer river cell locations

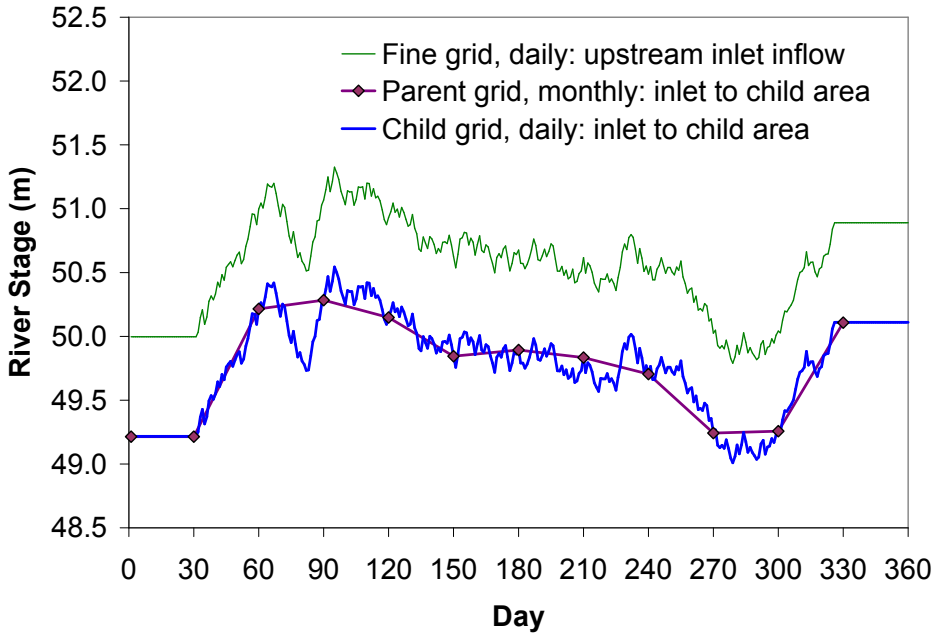

Figure 9. Stream-aquifer river stages

Table 2. Stream-aquifer grid resolutions, stress periods and time-steps

Grid Resolution	Stress Period Length	Number of Time-Steps per Stress Period
Globally Fine	1 Day	1
Globally Fine	1 Month	30
Globally Coarse	1 Day	1
Globally Coarse	1 Month	30
Coarse Parent with	Parent: 1 Month	30
Fine Child	Child: 1 Day	1

2.3.4 Model Analysis of Errors

Error analysis for this case study was made by comparing results of the globally fine daily model, which is considered to be the true results, with the results from the other simulations identified in Table 2. Several metrics were used to evaluate the relative accuracies of the various simulations compared to the true results, including the maximum head differences and the RMSEs of the head differences for three groups of observations. The first group of observations consists of the heads in the refined child area, the second group consists of the river cell nodes of the parent area, and the third group is comprised of the river cell nodes of the child area.

There are 418 observation node cells in the refined area and 601 river cell observation nodes, which are distributed as follows:

- 16 coarse grid river cell nodes in the parent area,
- 26 coarse grid river cell nodes in the child area,
- 169 fine grid river cell nodes in the parent area,
- 292 fine grid river cell nodes in the child area, and
- 98 child grid river cell nodes in the child area.

2.4 Rincon Valley Field Application Test Case

The site for the field application test case was located in the Rincon Valley irrigated corridor of the Lower Rio Grande River in southwest New Mexico. Figure 10 shows the general location of the study area in New Mexico.

The specific area of interest for this test case extends from below Caballo Reservoir to Seldon Canyon. A topographic map of this area is given in Figure 11. This figure shows the level land area adjacent to the river that supports agriculture in the valley. To irrigate this area, water is released from Caballo Reservoir in amounts partially based on ‘orders’, or requests for specific amounts of water, placed by the farmers in this valley. To determine how much water to release from Caballo, the amount of the orders must be increased to account for various gains and losses of the water as it transits from the reservoir to the farms. The main sources of losses include evaporation from the water surface, evapotranspiration due to the riparian vegetation, and seepage from the unlined river and canal network to, or from, the shallow unconfined aquifer.

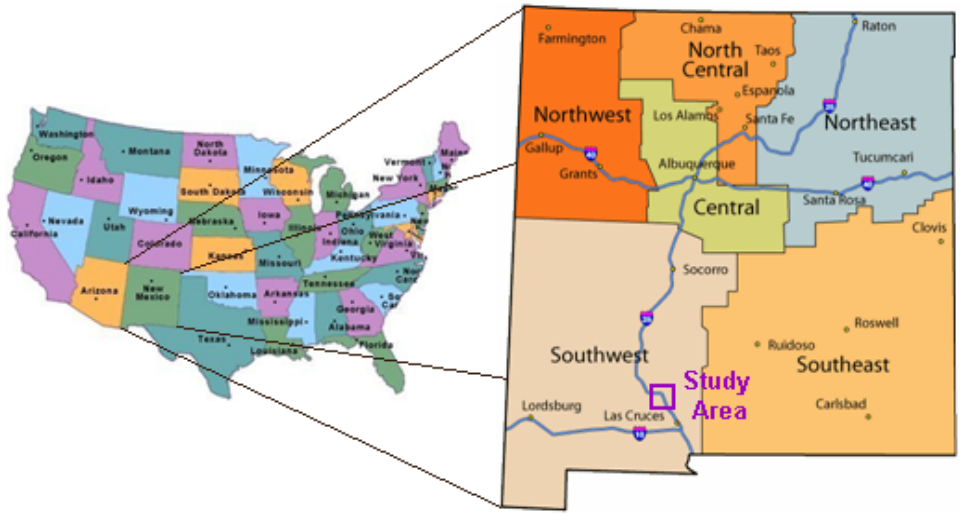

Figure 10. Rincon Valley field application study area

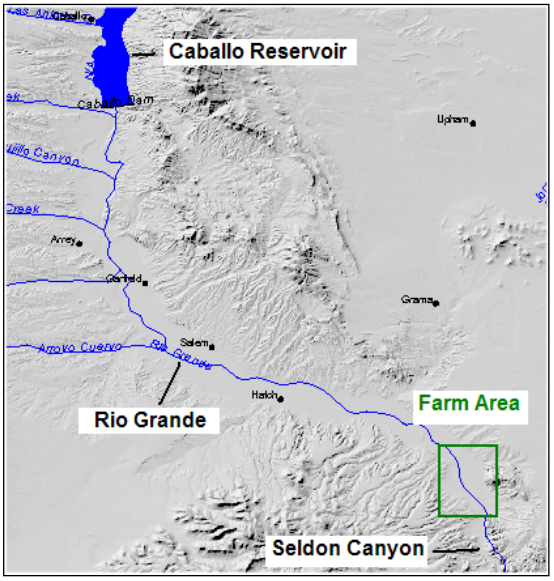

Figure 11. Topographic map of the Rincon Valley (from USGS 2008)

One relevant use of the LTS option of MODFLOW would be to quantify the amount of water gained, or lost, as stream and canal leakage to the aquifer. A regional model for this area exists, which has large variable-grid spacing, on the order of 800 to 1500 meters, with 2-stress periods per year (Weeden and Maddock, 1999). One stress period length is four months, extending during the non-irrigation season of November through February, and the second stress period length is eight months, to cover the irrigation season of March through October. One way to more efficiently manage the limited water resources in the arid southwest would be to improve

the estimates for stream leakage by having a daily stress-period model, especially during the irrigation seasons.

2.4.1 Weeden and Maddock Regional Model

Weeden and Maddock (1999) developed a MODFLOW-96 (Harbaugh and McDonald, 1996) regional groundwater flow model of the Rincon and Mesilla Valleys in New Mexico, which extended from Caballo Reservoir, to El Paso, TX. Their model was used as a base model for this field application, with the model domain truncated at Seldon Canyon to provide the regional coarse grid and coarse parent grid models of the Rincon Valley. This truncation was feasible since the Rincon Valley and the Mesilla Valley are physically separate groundwater systems divided by the Seldon Canyon area.

The original input data files were converted from the MODFLOW-96 format to the MF-LGR format. The smaller regional model of the Rincon Valley from Caballo Dam to Seldon Canyon was made by truncating the existing data files after row 50 and column 39, and the truncated Streamflow Routing Package data file (.STR) was converted to the .RIV River Package file format. The telescopic mesh programs (Leake and Claar, 1999) were updated for MF-LGR file formats, and then used to create the initial child grid model from the truncated regional (parent) model.

The original data files were for the time period 1915 through 1995. Additional data for January 1996 through February 2004 were added, including diversions to the Arrey Canal and flow in the Rio Grande below Caballo Dam. This data was acquired as part of a data collection effort for surface water flow in the Lower Rio Grande (Brown et al., 2004). When data was missing for the Arrey Canal, it was assumed that the diversion to Arrey Canal was equal to 11% of the flow below Caballo. This was based on the typical historical relationship between flow below Caballo and diversion to Arrey Canal.

Precipitation data for 1996 through February 2004 that was added to the model was taken from the Las Cruces Plant Science Center website (NMSU, 2004). This data was used to extend the ET and recharge data. This extension of data was done by finding a historic year with a similar amount of precipitation for the year, then using the ET or recharge for that historic year for the new year.

The Rincon Valley field application simulates a shorter time period, from Nov. 2001 through Feb. 2004. To get the initial conditions for this test case, the truncated regional model was run for the years 1915- 2004, and the resulting heads for November 2001 were extracted to use as the starting heads.

2.4.2 Model Parameters

The model domain is 48,724.40 m in the x-direction and 66,596.91 m in the y-direction, with the origin for these directions at the lower left-hand corner of the domain, from a plan view. The boundaries for the coarse grid models are all considered to be no-flow boundaries. Contours for the initial heads of the coarse grid models are shown in Figure 12.

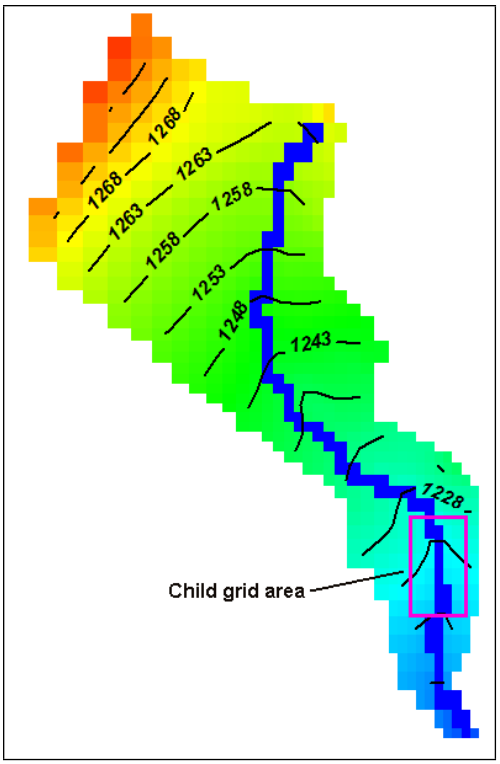

Figure 12. Initial head contours (m) for coarse/parent grid models

2.4.3 Model Grid Discretization

Two sets of grid discretizations were used for this test case, a globally coarse grid which is also used for the parent grid, and the refined grid in the child area of the model domain.

Globally Coarse and Parent Grids: The first grid resolution is for a globally coarse grid model and for the coarse parent grid of the refined child grid model. These coarse grids have 50 rows at non-uniform lengths ranging from 804 to 2,022 m, and 39 columns with widths ranging from 803 to 2,615 m for a total row length of 66,596.91 m and total column width of 48,724.40 m. This grid has four layers, with the top layer specified as unconfined and the lower three layers designated as confined. The elevation at the top of layer 1 varies from 1291 m to 1210 m, and the elevation at the bottom of layer 1 varies from 1270 m to 1150 m. The elevation at the bottoms of layers 2 through 4 are specified as constant values, with the bottom of layer 2 at 1,000 m, the bottom of layer 3 at 920 m and the bottom of layer 4 at 700 m. The refined child grid is located within the rectangle defined by corners at row 37, column 28, and at row 43, column 34.

Refined Child Grid: The second grid resolution is for the refined, child grid around a farm area. The child grid is a 7:1 ratio refinement of the coarse parent grid, and has 43 rows at lengths varying from 170 to 215 m, 43 columns at a width of 114.74 m each, for a total row length of 8251.36 m and a total column width of 4933.592 m. Only the first layer from the coarse grid/parent model was included in this model.

2.4.4 Model Time Resolutions

There are five stress-periods included for the coarse grid/parent models. These stress-periods cover the time period from Nov. 1, 2001 to Feb. 28, 2004 and are divided into non-irrigation and irrigation seasons as follows:

- Stress-period 1: Non-irrigation season from Nov. 1, 2001 to Feb. 28, 2002;
- Stress-period 2: Irrigation season from Mar. 1, 2002 to Oct. 31, 2002;
- Stress-period 3: Non-irrigation season from Nov. 1, 2002 to Feb. 28, 2003;
- Stress-period 4: Irrigation season from Mar. 1, 2003 to Oct. 31, 2003; and,
- Stress-period 5: Non-irrigation season from Nov. 1, 2003 to Feb. 28, 2004.

Stress-periods 1, 3 and 5 have 120 time-steps of one day each, and stress-periods 2 and 4 have 245 time-steps of one day each. The child grid has a total of 850 stress periods, with 1 daily time-step each. To create data for these stress-periods, daily flow data for the Rio Grande at Tonuco Bridge, Arrey Canal, and the Rincon Drain were used.

The daily flow data was extracted from the data acquired as part of a data collection effort for surface water flow in the Lower Rio Grande (Brown et al., 2004). Since the MF-LGR only supports the River package for streams that cross the child grid boundary, the flow data was converted to stage data assuming rectangular cross-sections. The stage data for Arrey Canal was then divided by four to represent the stage at the Rincon Lateral. The daily and seasonal stage data at the inlet to the child grid area are shown in Figure 13 for the Rio Grande, Figure 14 for the Rincon Lateral and Figure 15 for the Rincon Drain. These figures graphically show that the seasonal values cannot represent the variation of stage, and therefore cannot represent stream leakage on a daily basis during the irrigation season.

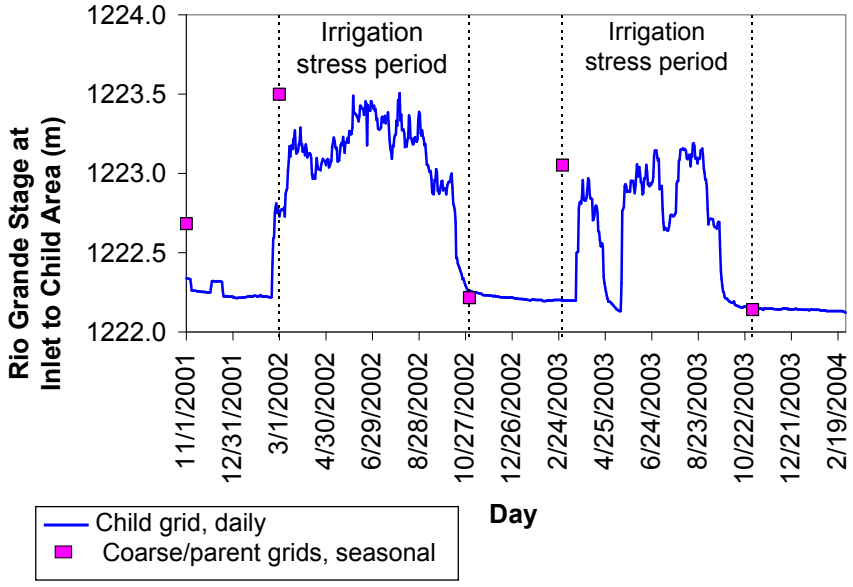

Figure 13. Stage data for the Rio Grande at the inlet to the child grid area

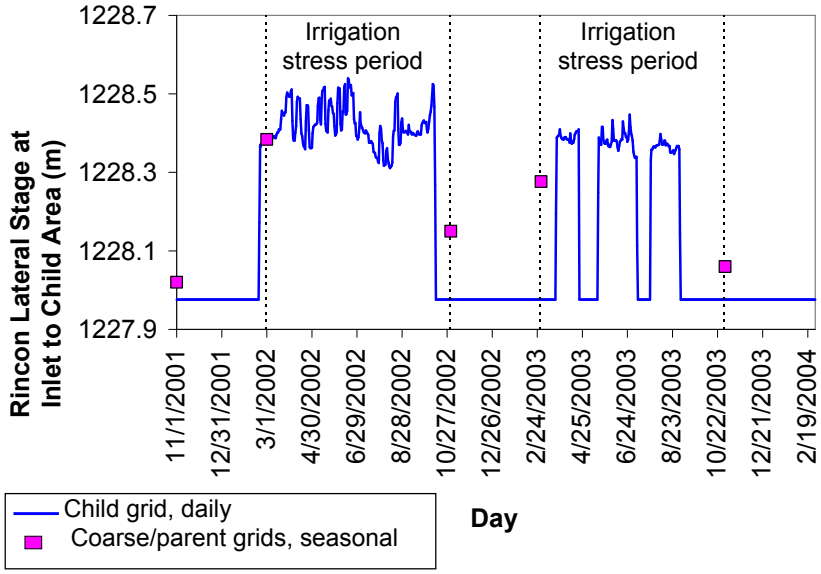

Figure 14. Stage data for the Rincon Lateral at the inlet to the child grid area

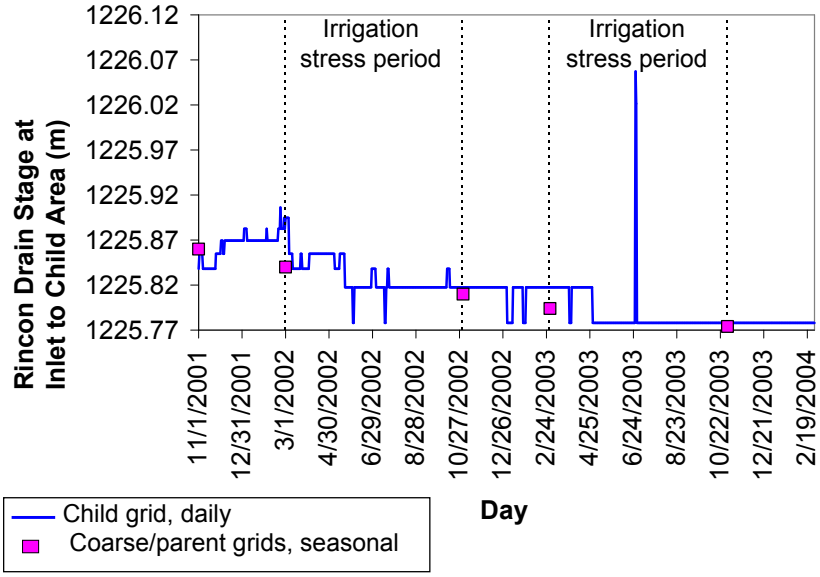

Figure 15. Stage data for the Rincon Drain at the inlet to the child grid area

3. RESULTS

3.1 Dual Well Test Case

Several aspects of the results from the dual well simulations were analyzed in order to evaluate the accuracy and efficiency of using the Local Time Stepping (LTS) model construct as compared to a variety of standard MODFLOW model constructs. These aspects and analyses of the results are discussed in the following sections.

3.1.1 Head Results at Well 1

In order to evaluate the accuracy of the heads resulting at Well 1 due to pumping, these heads were plotted for all of the simulations over the time period of the simulations, as shown in Figure 16. From this figure it is clear that the only simulation with head results comparable to the true results is the LTS simulation.

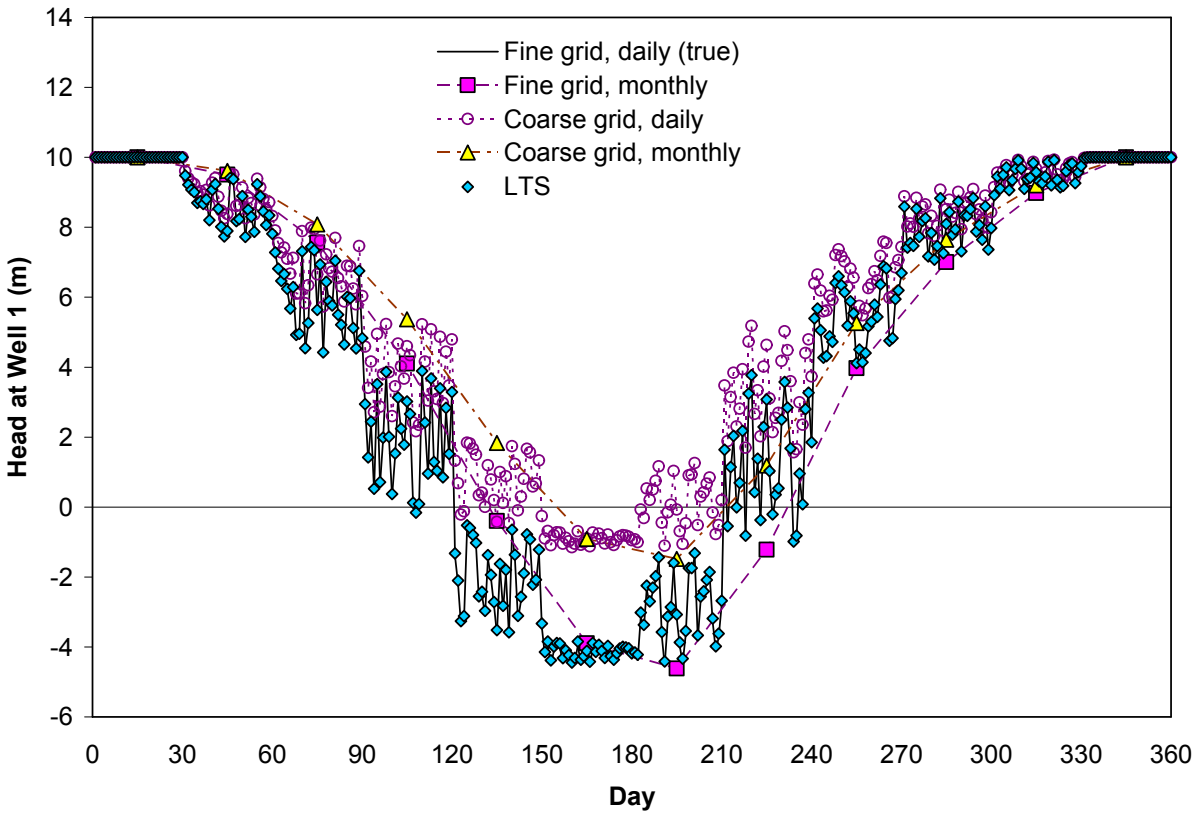

Figure 16. Heads from all simulations at Well 1

This is seen more clearly in Figure 17, which shows the true head values as the solid line, with the diamond markers representing the heads from the LTS child model. The locations of the

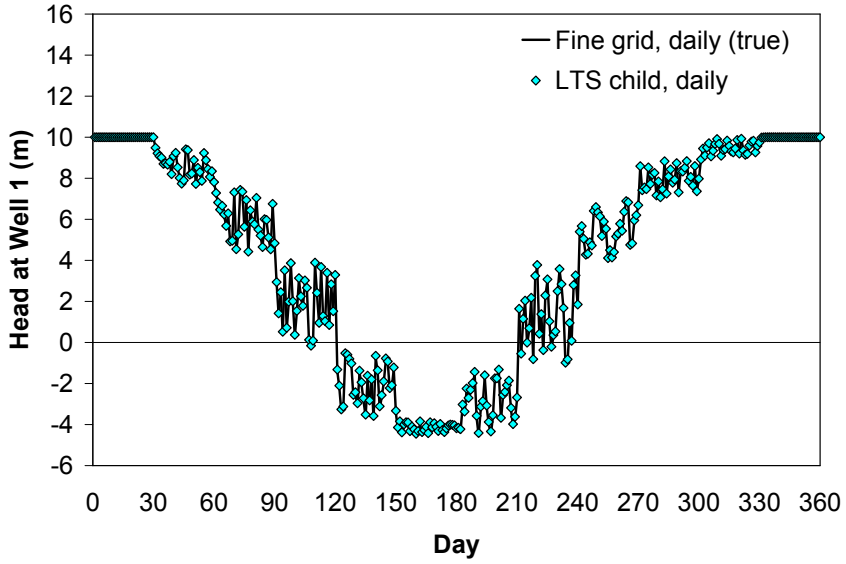

Figure 17. LTS child heads at Well 1

diamond markers are indistinguishable from the solid line, so a time-slice from day 120 to day 210 was extracted and graphed to show how close the agreement in heads is during the time of maximum drawdown. Figure 18 gives this time slice and shows how close indeed are the heads from the LTS child simulation and the true simulation.

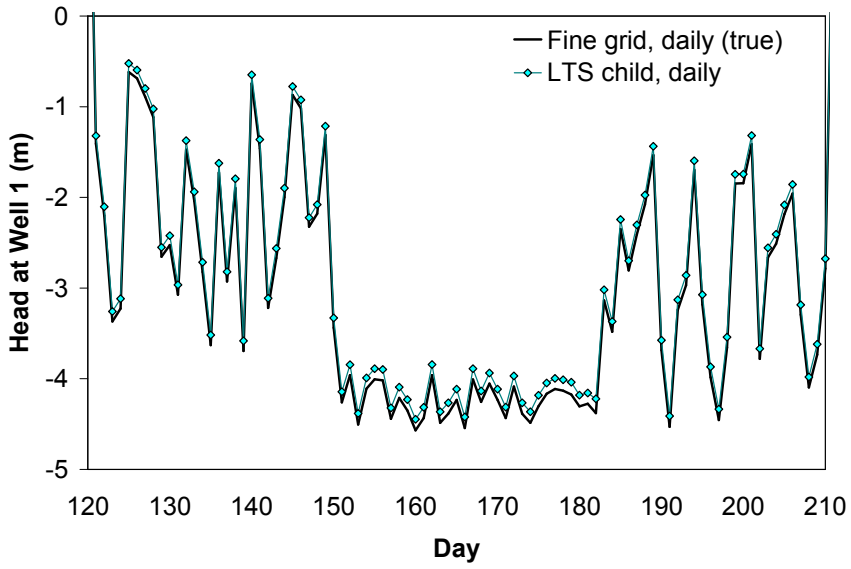

Figure 18. Time slice of LTS child heads at Well 1

3.1.2 Statistics for Results at Well 1

To further evaluate the accuracy of the heads resulting at Well 1 due to pumping, comparisons of two metrics were made for each of the simulations relative to the true solution. The metrics evaluated were the maximum head difference at the well and the RMSE of the head errors at the well. In order to visualize the relative magnitudes of these metrics, separate graphs were created for each metric, which show that the LTS simulation has the smallest (i.e. best) results in both categories and the monthly coarse grid simulation has the largest (i.e. worst) results.

The maximum head differences at the well for each simulation in relation to the true head results at this well are shown in Figure 19. The maximum head difference for the LTS simulation is -0.16 m, while the absolute maximum head differences for the other simulations range from 2.47 m to -3.94 m. These values are large enough to render the results from these simulations of questionable value, while the LTS value is very small indicating that the results from that simulation are quite accurate and useful.

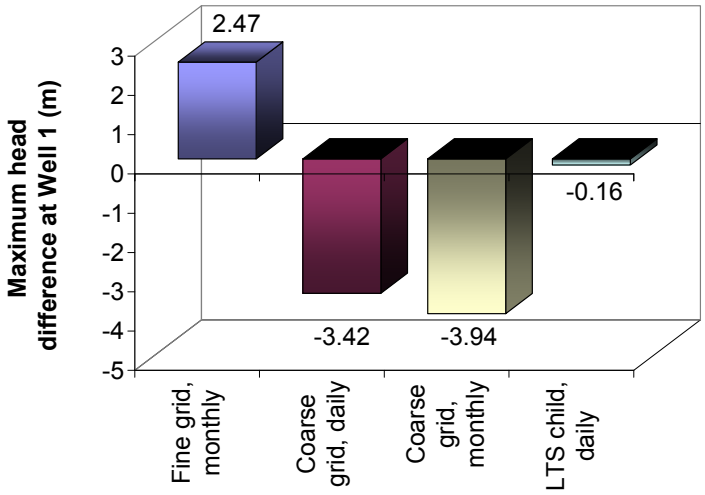

Figure 19. Maximum head differences at Well 1

Figure 20 shows the RMSE of the head differences at Well 1 compared to the true head values at this well. The LTS RMSE is 0.06, which indicates very small error in the head differences for this simulation, while the RMSEs for the other simulations range from 1.40 to 1.98. The relative values of these RMSEs are much higher than the RMSE of the LTS simulation, which means the average error of the other simulations is very high.

Based on these metrics for head at Well 1, it is clear the LTS simulation has the most accurate results and is suitable for modeling drawdown at the pumping wells.

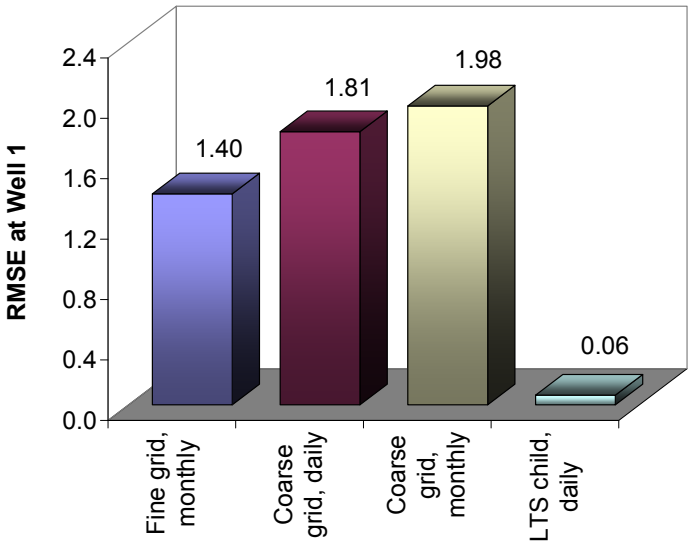

Figure 20. RMSEs of heads at Well 1

3.1.3 Maximum Head Differences at Observation Nodes

The maximum head differences for each simulation for the observation nodes in the parent grid area are presented graphically in Figure 21, and shows that the LTS parent and daily coarse grid simulations have the smallest head differences. The maximum head difference for both simulations is -0.11 m on day 180, at the time of maximum drawdown. The head differences for the monthly fine grid simulation range from -1.18 m on day 150 to 1.34 m on day 240. The monthly coarse grid simulation head differences are quite close to the head differences for the monthly fine grid simulations. The head differences for these simulations range from -1.17 m at day 150 to 1.47 m at day 240.

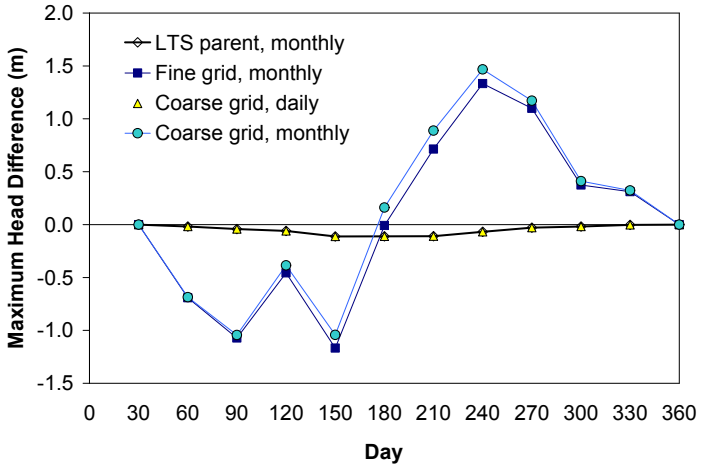

Figure 21. Dual well maximum head differences in parent grid area

The maximum head differences for each simulation for the observation nodes in the child grid area around Well 1 are presented graphically in Figure 22 and these results are almost identical to the results from the parent area as to the patterns of the head differences. The main dissimilarity is that the magnitude of the head differences is larger in the child area. The LTS simulation has a maximum head difference of -0.125 and the daily coarse grid simulation has a maximum head difference of -0.17 m, while the monthly fine grid simulation ranges from -1.80 m to 1.88 m, and the monthly coarse grid simulation ranges from -1.63 m to 2.06 m.

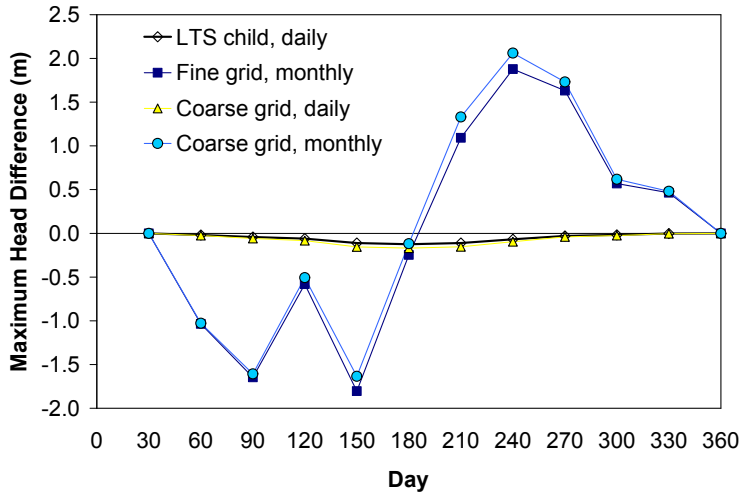

Figure 22. Dual well maximum head differences in refined grid area

In general, these graphs show that the errors in both the parent and the child areas are much larger for the global grid simulations with monthly stress-periods, than for the LTS and daily stress-period simulations.

3.1.4 RMSEs at Observation Nodes

The RMSEs for the head differences in the parent area of each simulation at the observation nodes are presented graphically in Figure 23, and the patterns in this graph are much the same as for the maximum head differences in the parent area. The LTS and daily coarse grid simulations have the smallest RMSEs, with a maximum RMSE of 0.12 on day 180. The maximum RMSE for the monthly fine grid simulation is 0.99, and the maximum RMSE for the monthly coarse grid simulations is 1.10.

The RMSEs of the head differences for each simulation at the observation nodes in the child grid area around Well 1 are presented graphically in Figure 24, and again, the results for the child area are very similar to the results from the parent area, however the magnitude of the RMSEs in the child area are larger. The LTS and daily coarse grid simulations have approximately the same RMSE of 0.12, while the maximum RMSE for the monthly fine grid simulation is 1.38 and the maximum RMSE for the monthly coarse grid simulation is 1.51.

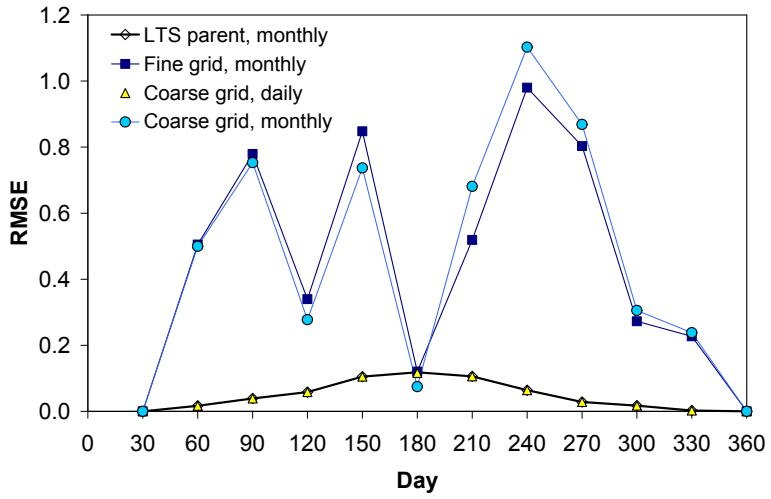

Figure 23. Dual well RMSEs of heads in parent grid area

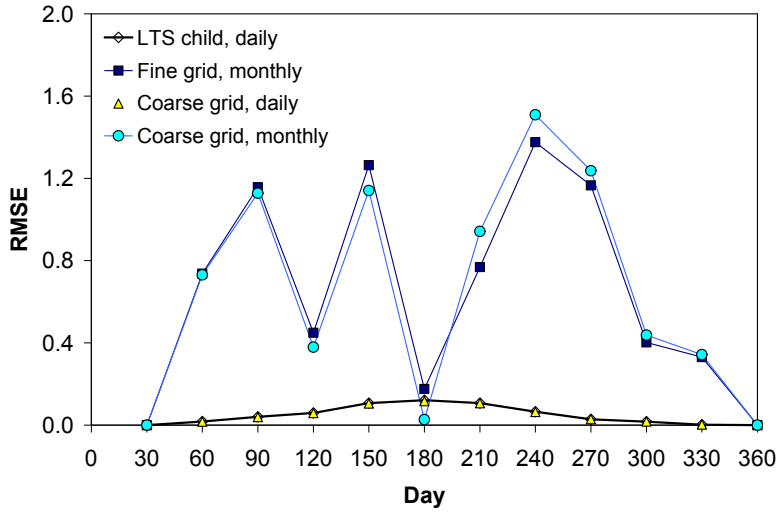

Figure 24. Dual well RMSEs of head in refined grid area

Overall, these graphs show that the average head error in both the parent and child areas is very small and quite acceptable for the LTS and daily coarse grid simulations. However, the errors for the monthly simulations are quite large and indicate the results from these simulations may not be valid. It should be noted that although this metric shows an overall small error for the daily coarse grid simulation, the previous comparison of the heads at the well node indicated that this simulation does not accurately represent the drawdown in the well. At the time of maximum drawdown, the head was several meters higher than the true head at the well.

3.1.5 Dual Well Run Times

The simulations for this research were run on a COMPAQ HP PC laptop computer, with an AMD Athlon 64 Processor at 1.99 GHz and 2.00 GB of RAM. The operating system was Microsoft Windows XP, Version 2002, and Service Pack 2. The computer run times for the dual well simulations are given in Figure 25. The globally coarse grid simulations had the shortest run times, and were also found to have correspondingly the largest errors in drawdown at the wells. The monthly fine grid simulation had the next fastest run times, but also had poor results for drawdown at the wells.

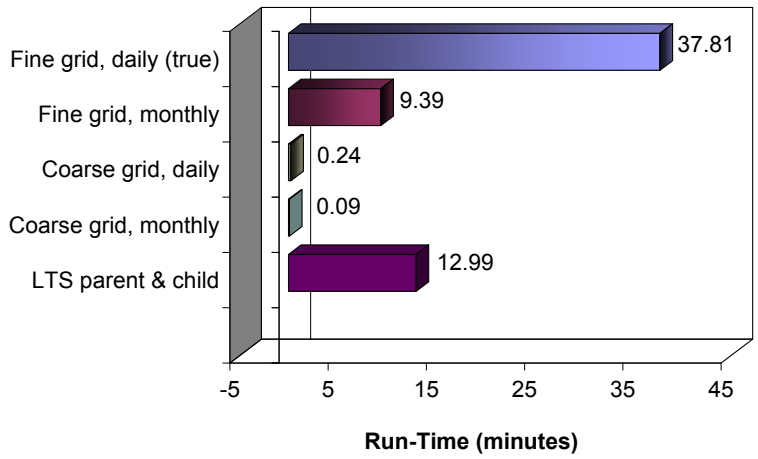

Figure 25. Dual well run times

As expected, the daily fine simulation takes the longest to run, with the LTS simulations taking about one-third as long to run. The results from the LTS simulation compare favorably with the true results, and therefore the LTS simulation provides a viable solution with a substantial savings in time.

To further reduce the run time required for the LTS simulation, designing the model domain such that the head at the boundaries of the refined area do not change greatly during the course of the simulation would reduce the number of iterations required for the LGR solution, with an overall reduction in the time required to run the simulation. The head at the boundaries of the refined areas for this test case drop nearly six meters during the simulation, which requires many iterations of the LGR solution for each child grid stress-period. Moving these boundaries further out from the wells would greatly increase the efficiency of the LTS solution.

3.2 Stream-Aquifer Test Case

Several aspects of the results from the stream-aquifer simulations were analyzed in order to evaluate the accuracy and efficiency of using the LTS model construct as compared to a variety

of standard MODFLOW model constructs. These aspects and analyses of the results are discussed in the following sections.

3.2.1 Maximum Head Differences at Observation Nodes

The maximum head differences for each simulation at the observation nodes in the child grid area are displayed in Figure 26, and shows that the LTS child daily simulation typically has the smallest head differences, followed by slightly larger head differences for the monthly fine grid and daily coarse grid simulations. The maximum head differences for the LTS simulation range from 0.69 m on day 60 to -0.33 m on day 270. These days correspond respectively to times when the stage in the river rises and drops steeply. The head differences for the monthly fine grid and daily coarse grid simulations have head differences ranging from 0.96 m on day 60 to -0.57 m on day 270. The monthly coarse grid simulation has the largest head differences, which range from 1.04 m at day 60 to -1.24 m at day 270.

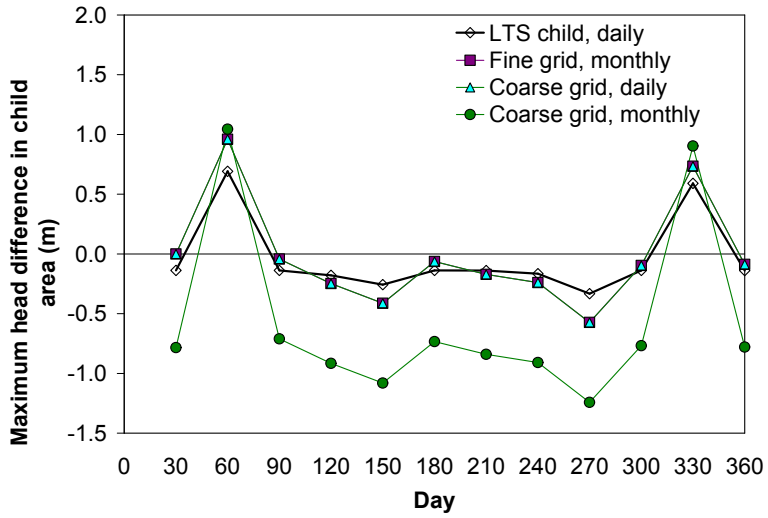

Figure 26. Stream-aquifer maximum head differences in child area

The maximum head differences for the river cell nodes in the parent area of the model domain are presented graphically in Figure 27, and indicates that the head differences in the parent area are very similar for all simulations, with the monthly fine grid and daily coarse grid simulations generally showing the smallest head differences. The largest head differences for the river cells in the parent area range from 1.11 m at day 60 to -0.58 m at day 270 for the monthly coarse grid simulation.

The maximum head differences for the river cell nodes in the child area of the model domain are presented graphically in Figure 28, and shows that the LTS simulation has the smallest range of head differences, extending from 0.65 m on day 60 to -0.48 m from days 90 to 300, for a total range of 1.13 m. In contrast, the monthly fine grid and daily coarse grid simulations range from

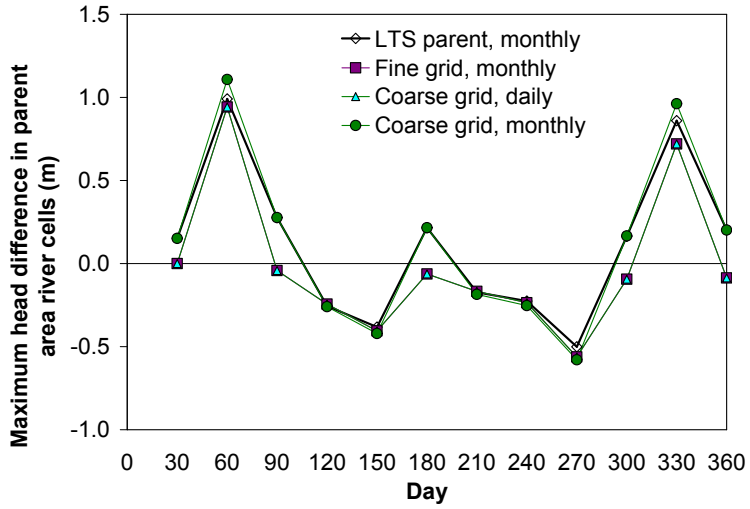

Figure 27. Stream aquifer maximum head differences in parent area river cells

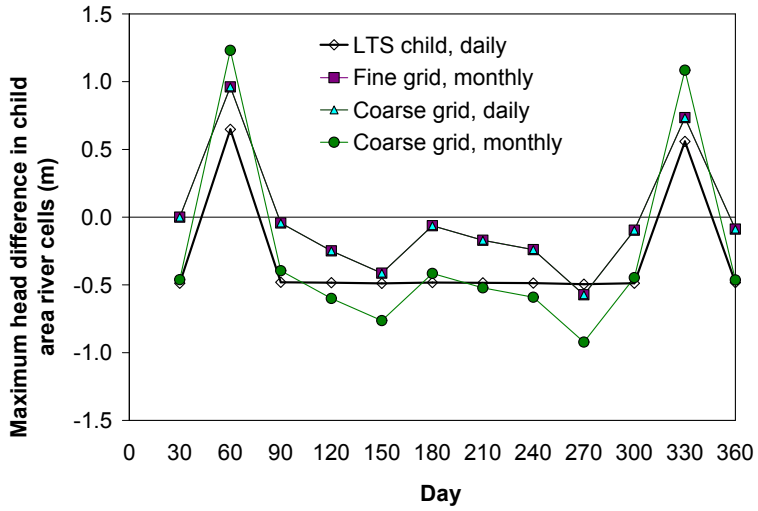

Figure 28. Stream-aquifer maximum head differences in child area river cells

0.96 m on day 60 to -0.57 m on day 270, for a span of 1.53 m; and the monthly coarse grid simulation ranges from 1.23 m on day 60 to -0.92 m on day 270 for a total difference of 2.15 m.

Overall, the maximum head difference data shows that the LTS simulation has the smallest differences in the refined area, which is the area of interest, and the monthly coarse grid simulation has the largest head differences in both the parent and child areas.

3.2.2 RMSEs at Observation Nodes

The RMSEs for the head differences in the refined child area of each simulation are displayed graphically in Figure 29 and shows that the RMSEs for the LTS simulation are much smaller than for the other three simulations with a maximum RMSE of 0.182 on day 60. The maximum RMSE for the monthly fine grid simulation is 0.844, for the daily coarse grid simulation is 0.8889, and for the monthly coarse grid simulation is 0.7164.

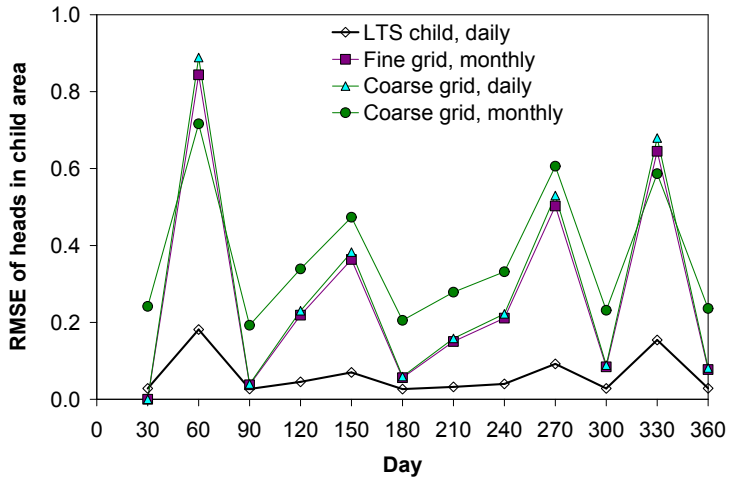

Figure 29. Stream-aquifer RMSEs of heads in child area

The RMSEs of the head differences for the river cells in the parent area are plotted in Figure 30, and indicates that these RMSEs are all quite similar, with the LTS simulation RMSEs slightly lower than for the other simulations.

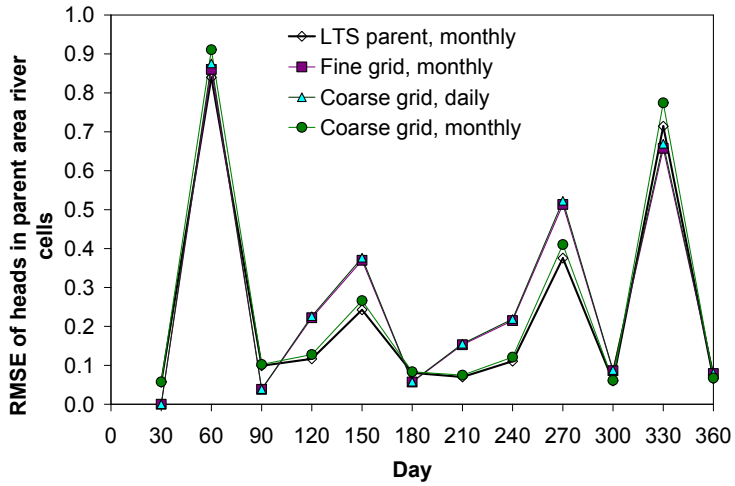

Figure 30. Stream-aquifer RMSEs of heads in parent area river cells

The RMSEs of the head differences for the river cells in the child area are graphed in Figure 31, showing that the RMSEs for the LTS simulation are much lower than for the other simulations, remaining near 0.1 for the duration of the simulation. The maximum RMSE for the monthly fine grid simulation is 0.93 on day 60, for the daily coarse grid simulation is 0.93 on day 60, and for the monthly coarse grid simulation is 0.98, also on day 60.

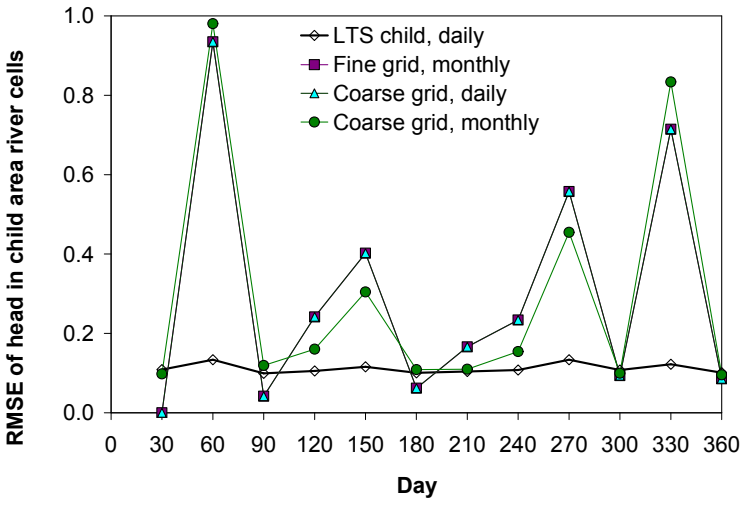

Figure 31. Stream-aquifer RMSEs of head in child area river cells

The results show that the RMSEs for the LTS simulation in the refined area are much lower than for any of the other simulations, and that in the parent area the RMSEs are similar for all simulations.

3.2.3 Stream-Aquifer Run Times

The computer run times for the stream-aquifer simulations are given in Figure 32 and show that the globally coarse grid simulations have the shortest run times, followed by the monthly globally fine grid simulation and the LTS simulation. The daily globally fine simulation takes the longest to run with the LTS simulations taking about one-sixth as long to run.

To further reduce the run time required for the LTS simulation, designing the model domain such that the head at the boundaries of the refined area do not change greatly during the course of the simulation would reduce the number of iterations required for the LGR solution. This would lead to an overall reduction in the time required to run the simulation.

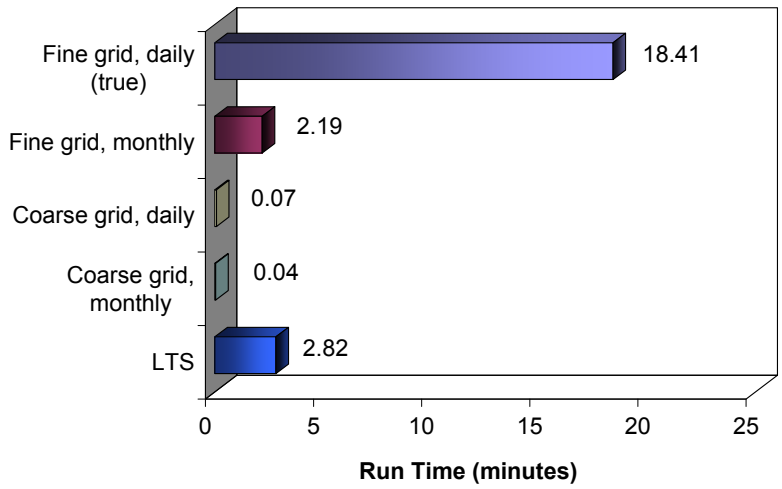

Figure 32. Stream-aquifer run times

3.3 Rincon Valley Field Application Test Case

In order to verify the results from the field application models, results from a regional model of the Lower Rio Grande (LRG) Basin developed by S.S. Papadopulos & Associates (S.S. Papadopulos 2007) for the New Mexico State Engineer was used as a baseline for leakage comparisons. This regional model was developed for the state as a tool to be used in administrating water rights and for applying active water management.

As previously stated, the results of interest for the Rincon Valley field application are the stream leakage values between the river/canal network and the unconfined aquifer. Table 3 gives the total leakage volumes at the seasonal stress period intervals for the combined results of the LTS child and parent grid model, for the coarse grid model, and for the LRG 2007 regional model.

Table 3. Rincon Valley seasonal stream leakage volumes

Date	Season	LTS (m^3)	Coarse Grid (m^3)	LRG 2007 (m^3)
2/28/2002	Non-irrigation	-20,525,568	-16,845,469	-16,087,034
10/31/2002	Irrigation	25,186,924	15,944,621	18,981,687
2/28/2003	Non-irrigation	-19,538,452	-12,902,448	-18,636,509
10/31/2003	Irrigation	33,127,624	28,047,040	27,123,074
2/28/2004	Non-irrigation	-14,316,044	-7,622,624	-7,641,014

These leakage values are also shown graphically in Figure 33, and show close agreement between the three models for total leakage volume per season. Figure 34 shows the daily variations in stream leakage for the LTS child model, and together with Figure 33 show how

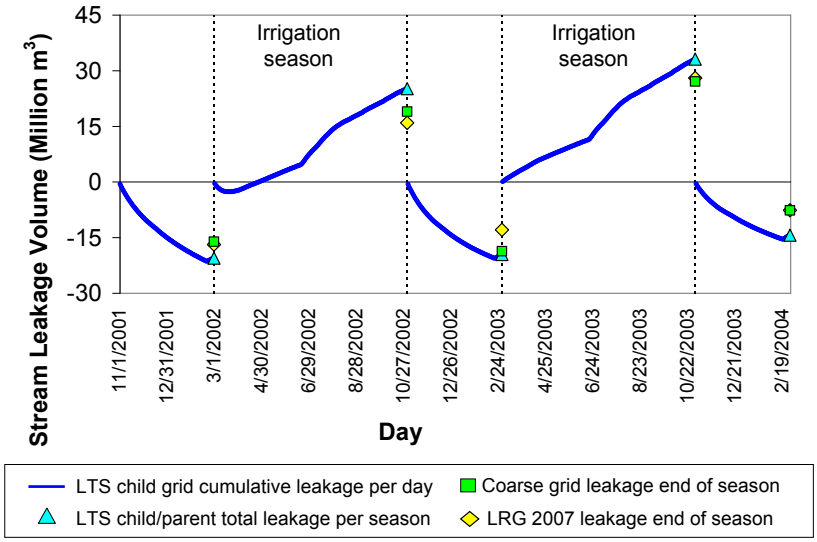

Figure 33. Rincon Valley stream leakage comparisons

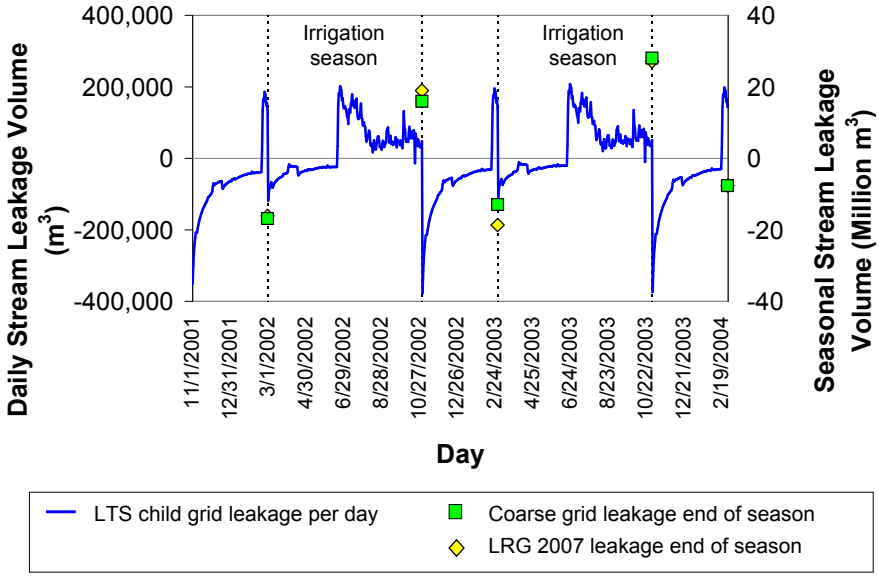

Figure 34. Rincon Valley stream leakage volumes

variable the stream leakage is on a daily basis. This confirms the supposition that seasonal stream leakage values cannot capture this variation nor provide information useful for daily operations of an irrigation system.

Figure 35 shows the daily stream leakage rate in cubic feet per second (cfs) for the LTS child model, and the average leakage rate per season. These average leakage rates range from a gain of 28 cfs during the low flow non-irrigation seasons to a loss of 13 cfs during the irrigation

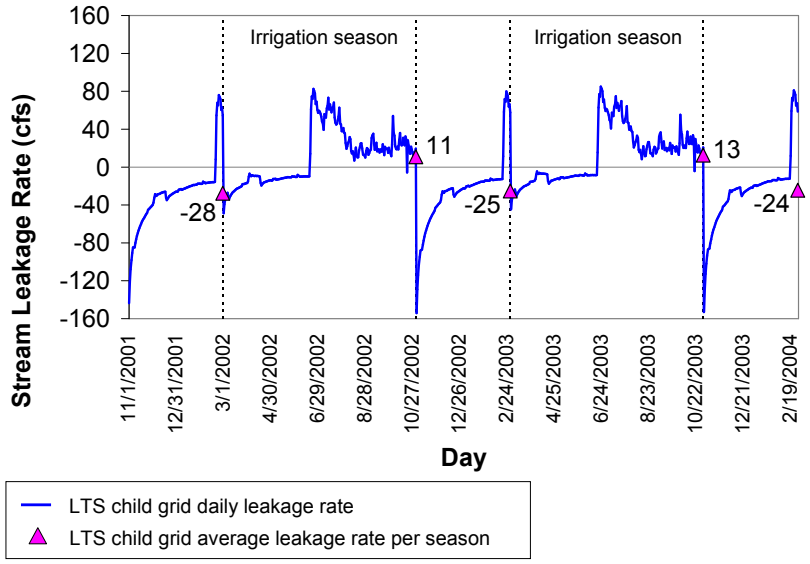

Figure 35. Rincon Valley child grid stream leakage rates

seasons. The general magnitude of the gains are confirmed by a study done by S.S. Papadapolus during the low flow times of January 1995, 1997, 1999 and 2000 (S.S. Papadapolus 2007). They found that the net gain in the river between Caballo Reservoir and Leasburg Dam (which is just below Seldon Canyon) is on the order of 35 to 50 cfs.

Additional verification of the model leakage rates during the low flow season came from a loss study based on Elephant Butte Irrigation District (EBID) meter notes for October 22-23, 2007 (EBID, personal communication, 29 July 2008). At the end of the 2007 irrigation season EBID finished its allocated water and ceased diversions, while downstream the El Paso County Water Improvement District No. 1 (EPCWID) continued to release and divert water. This downstream diversion with no upstream diversion created an ideal setting for a loss study. During the study, a constant release from Caballo Dam was maintained for several days. No storm runoff events occurred during the study. EBID and EPCWID metered the flow repeatedly at several stations along the Rio Grande, including the river below Caballo Dam and at Hayner Bridge, just below the Rincon model study site. From these meterings, losses for the Rincon Valley reach were computed. A comparison of the results of this study with the Rincon model results is shown in Table 4. This comparison shows leakage rates with reasonably close values for Oct. 22, and almost identical values for Oct. 23.

Table 4. Leakage rate comparisons

	Leakage Rate (cfs) Oct. 22	**Leakage Rate (cfs) Oct. 23**
Rincon Model (2002)	46	38
Rincon Model (2003)	51	43
EBID Loss Study (2007)	29	38

Several head contours for the child grid area of the Rincon Valley are used to confirm the validity of the LTS model system in relation to the coarse grid model, and show the changes in head that occur in the child grid model that cannot be captured by the coarse grid model. Figure 36 shows the head contours in the child area at (a) the end of the first non-irrigation stress period, after 120 days of simulation and (b) after the second stress period, which was an irrigation stress period of 245 days.

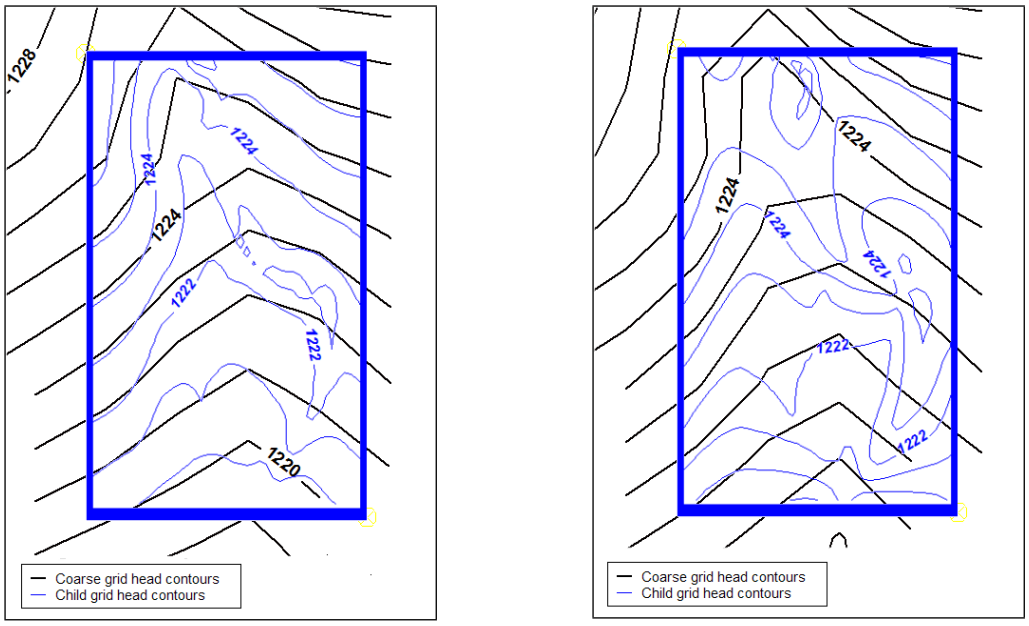

(a) After 120 days (b) After 365 days

Figure 36. Head contours for child grid area after (a) 120 days and (b) 365 days

This figure shows that the LTS child and coarse grid heads at the boundaries of the child grid match quite closely, and that after 120 days with little or no stresses on the system, the contours of the two models in the interior of the child grid area remain fairly consistent. Both sets of contours indicate that the river at this time is a gaining stream. After 365 days at the end of an irrigation stress period, the heads at the child grid boundaries remain close, but the contours within the boundary are vastly different. The coarse grid head contours still indicate a gaining stream system, while the LTS child grid head contours are indicative of a losing stream system.

Figure 37 shows these head contours at (a) the end of the second non-irrigation stress period, where both the LTS child and coarse grid heads contours return to similar conditions and both indicate a gaining stream system. At (b) the end of the second irrigation stress period, the head contours are similar to the contours after the first irrigation stress period. The coarse grid contours still indicate a gaining stream condition, while the LTS child grid contours are more complicated, but are more indicative of a losing stream system.

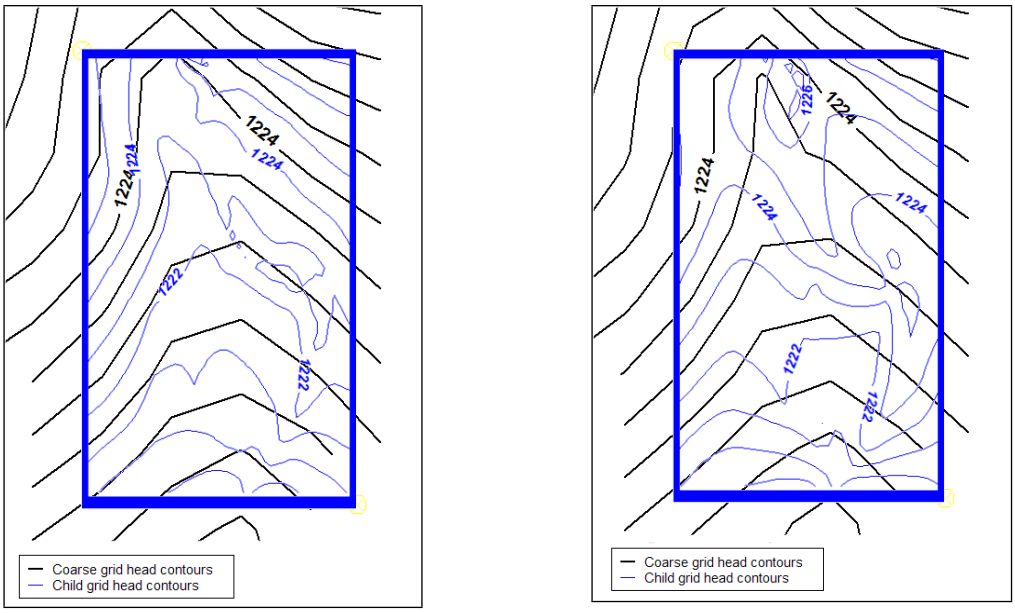

(a) After 485 days (b) After 730 days

Figure 37. Head contours for child grid area after (a) 485 days and (b) 730 days

These contour diagrams confirm the conclusions from the stream leakage data, that the coarse grid model cannot accurately reflect the changing conditions in the refined area, especially during the irrigation seasons. One reason for the greater variability of the child grid model results can be found by comparing the head contours and river grid cells in the refined area of the coarse grid model with the child grid model. Figure 38 shows these contours and river grid cells at the end of the first irrigation stress period, with figure (a) representing the child region of the coarse grid model and (b) representing the refined child grid model.

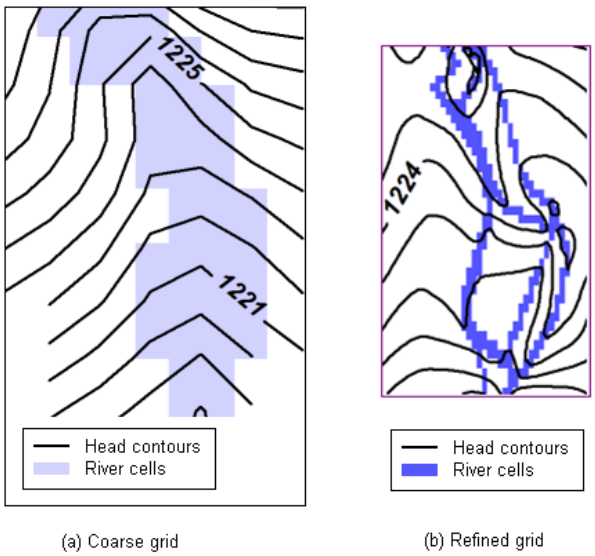

(a) Coarse grid (b) Refined grid

Figure 38. Compare contours and river grid cells for (a) coarse grid and (b) refined grid

These figures clearly show that the head contours of the refined grid follow the river cells which are small enough to represent separate stream entities, while the river cells of the coarse grid are quite large and blend together resulting in much less variability of the head contours.

4. SUMMARY AND CONCLUSIONS

Local Time-Stepping for surface/ground water interactions using MODFLOW-LGR with multiple-area grid refinement adds the capability to specify different stress period lengths for the coarse parent grid and the refined child grids. Implementing this option in the standard MODFLOW software allows users already familiar with MODFLOW a seamless transition to developing models that incorporate local time-stepping. All of the standard MODFLOW packages are supported, however only the RIVER package may be used for streams that cross the boundary between the parent grid and a child grid. If a stream is completely specified within the refined area, then any of the stream flow routing packages may be used.

There are no additional input instructions or directions beyond those specified for the LGR option, and the only constraints are that the stress periods of the refined models must coincide with the time-steps of the coarse model (i.e. the total number and length of the refined model stress periods must match exactly the number and length of the coarse model time-steps), and the refined model stress periods may only have one time-step.

Three test cases were examined, and in general, the results from two LTS hypothetical test case simulations provide good accuracy in the refined area when compared to the true results, and run three to six times faster than a globally fine grid simulation. The results from the field application test case showed that more detailed leakage information may be obtained from the LTS simulation, which could be extremely valuable in scheduling daily operations of an irrigation system.

4.1 Dual Well Test Case

The first hypothetical test case was a dual well system with two refined areas and five different combinations of grid spacing, stress period length and time-step size. This system did not include any vertical refinement of the single layer of the system. The metrics examined for the dual well test case showed that the head at the pumping wells was very well simulated by the LTS option with a maximum head difference of -0.16 m. The other simulations compared poorly with the true head at the wells, with maximum head differences ranging from 2.47 m for the monthly fine grid simulation to -3.94 m for the monthly coarse grid simulation. These head differences at the wells are confirmed by the RMSE error statistics. The RMSE of the heads at the wells is 0.06 for the LTS simulation, and varies from 1.40 to 1.98 for the other simulations. It is clear from these results that only the LTS simulation provides comparable and acceptable values of head at the wells.

Observation nodes were established for the dual well test case, with one group of observation nodes in the coarse parent area and the second group of observation nodes located in the refined child area around Well 1. The maximum head differences for the LTS simulation and the daily

coarse grid simulation in both the parent and child areas were very much smaller than the corresponding head differences for the other simulations. The largest head difference for the LTS simulation in the parent area was -0.11 m, and in the child area was -0.13 m. This contrasts to the maximum head differences of the other simulations ranging from 1.47 m to -1.17 m in the parent area, and 2.06 m to -1.8 m in the child area. The RMSEs of the LTS and daily coarse grid simulations are very small, with the largest RMSE at 0.116 in the parent area, and 0.1164 in the child area. The largest RMSE of the other simulations is 1.1 in the parent area and 1.51 in the child area.

These statistics for the dual well system show that the LTS simulations provide very good results in both the parent and child areas of the model domain. At the same time, the LTS simulation for this scenario runs three times faster than the daily globally fine grid simulation. An even greater improvement in the run-time of the LTS simulation could be achieved by moving the boundaries of the refined area farther out to a location where the head changes at the boundary are very small.

4.2 Stream-Aquifer Test Case

The second hypothetical test case was a stream-aquifer system with one refined area and five combinations of grid spacing, stress period length and time-step size. This test case included two levels of vertical refinement, with nine fine grid layers combined into three layers for the coarse grid, and the three coarse grid layers divided into five layers for the refined grid. The stream-aquifer test case compares the results of simulations for a meandering stream hydraulically connected to an aquifer. Several groups of observation nodes were established with one group of observation nodes in the refined child area, and the other groups of nodes consisting of river cells in both the parent area and the child area for the fine and coarse grids.

The maximum head differences for the LTS simulation in the child area were smaller than the corresponding head differences for the other simulations. The largest head difference for the LTS simulation was 0.69 m. This is close to one-half of the maximum head differences of the other simulations, which was -1.24 m. There was little difference in the maximum head differences in the river cell nodes of both the parent and child areas. The RMSEs of the heads in the refined area for the LTS simulations were very small, with the largest RMSE at 0.1815. The largest RMSE of the other simulations is 0.89 in the child area. The RMSEs of the heads in the parent area river cells are fairly similar for all simulations, but the RMSEs of the heads in the child area river cells is much smaller for the LTS simulation, remaining around 0.12 throughout the simulation.

These statistics for the stream-aquifer system show that the LTS simulations provide good results, especially in the child areas of the model domain. In contrast to the dual well test case where the globally fine grid and child grid row and column sizes are identical, the child grid rows and columns for the stream-aquifer test case were three times larger than the globally fine grid rows and columns. Better results for this test case could be obtained by designing the refined grid row and column sizes to be the same as the globally fine grid. The LTS simulation for this scenario runs approximately six times faster than the daily globally fine grid simulation, which could also be sped up by moving the boundaries of the refined area farther out.

4.3 Rincon Valley Field Application

The field application test case was for an irrigation system in the Lower Rio Grande river area of southwest New Mexico. This application included a regional coarse grid model with four aquifer layers, and one refined child grid model with a single unconfined aquifer layer surrounding a small farm area in the Rincon Valley. The coarse grid/parent model was designed to estimate conditions at the end of the winter non-irrigation stress periods, and at the end of the spring/summer irrigation stress periods. The LTS child simulation refined a portion of this model around a farm area at the southern end of the model area, and represented daily stress periods throughout the model period. The spatial discretization represented a 7:1 ratio of column and row sizes, and only included the top layer of the coarse grid model. The results from the field application show that using the LTS option for MF-LGR provides information on a daily basis, which may be useful for scheduling daily operations of the irrigation system. The stream leakage values were compared between the coarse grid, LTS and LRG 2007 models, and showed close agreement between the seasonal leakage volumes. Average leakage rates for the child grid area ranged from -28 cfs to 13 cfs which is consistent with leakage rates in this reach of the Rio Grande. Contour diagrams of head at the end of the seasonal stress periods indicated that the coarse grid model is not sensitive enough to reflect that the river system changes from a gaining to a losing stream system during the irrigation stress periods.

REFERENCES

Berger, J. J., and R. J. Leveque (1998), Adaptive mesh refinement using wave-propagation algorithms for hyperbolic systems, *SIAM Journal on Numerical Analysis, 35(6)*, 2298-2316.

Brown, C., Z. Sheng and M. Rich (2004), *Paso del Norte Watershed Council Coordinated Water Resources Database Project*, New Mexico Water Resources Research Institute and Texas Water Resources Institute, Technical Completion Report 327.

Chang, S., Y. Wu, V. Yang, and X. Wang (2005), Local time-stepping procedures for the space-time conservation element and solution element method, *International Journal of Computational Fluid Dynamics, 19(5)*, 359-380.

Crossley, A. J. (1999), Accurate and efficient numerical solutions for the Saint Venant equations of open channel flow, Thesis, University of Nottingham.

Crossley, A. J., N. G. Wright, and C. D. Whitlow (2003), Local time stepping for modeling open channel flows, *Journal of Hydraulic Engineering*, *129(6)*, 455-462.

Crossley, A. J., and N. G. Wright (2005), Time accurate local time stepping for the unsteady shallow water equations, *International Journal for Numerical Methods in Fluids*, *48*,775-799.

Harbaugh, A. W., and M. G. McDonald (1996), User's documentation for MODFLOW-96, an update to the U. S. Geological Survey modular finite-difference ground-water flow model, USGS, Open-File Report 96-485.

Harbaugh, A. W. (2005), MODFLOW-2005, the U.S. Geological Survey Modular Ground-Water Model – the ground-water flow process, *USGS Techniques and Methods 6-A16*, 9 chapters.

Hu, K., C. G. Mingham, and D. M. Causon (2006), A mesh patching method for finite volume modeling of shallow water flow, *International Journal for Numerical Methods in Fluids*, *50*, 1381-1404.

Imamura, T., K. Suzuki, T. Nakamura, and M. Yoshida (2005), Acceleration of steady-state lattice Boltzmann simulations on non-uniform mesh using local time step method, *Journal of Computational Physics*, *202*, 645-663.

Kirby, R. (2002), On the convergence of high resolution methods with multiple time scales for hyperbolic conservation laws, *Mathematics of Computation*, *72(243)*, 1239-1250.

Lackey, T.C., and F. Sotiropoulos (2005), Role of artificial dissipation scaling and multigrid acceleration in numerical solutions of the depth-averaged free-surface flow equations, *Journal of Hydraulic Engineering*, *131(6)*, 476-487.

Lamby, P., S. Müller, and Y. Stiriba (2005), Solution of shallow water equations using fully adaptive multiscale schemes, *International Journal for Numerical Methods in Fluids*, *49*, 417-437.

Leake, S.A., and D. V. Claar (1999), Procedures and computer programs for telescopic mesh refinement using MODFLOW, *USGS Open-File Report 99-238*, 61 p.

Mehl, S. W., and M. C. Hill (2005), MODFLOW-2005, The U.S. Geological Survey Modular Ground-Water Model – Documentation of the Multiple-Refined-Areas Capability of Local Grid Refinement (LGR) and the Boundary Flow and Head (BFH) Package, *USGS Techniques and Methods 6-A21*, 68 p.

Mehl, S.W., and M. C. Hill(2007), MODFLOW-2005, The U.S. Geological Survey Modular Ground-Water Model – Documentation of Shared Node Local Grid Refinement (LGR) and the Boundary Flow and Head (BFH) Package, *USGS Techniques and Methods 6-A12*, 13 p.

Niessner, J., and R. Helmig (2006), Multi-scale modeling of two-phase-two-component processes in heterogeneous porous media, submitted to *Numerical Linear Algebra with Applications*.

NMSU State Climate Network (2004), Las Cruces Plant Science Center Website, http://weather.nmsu.edu/cgi-shl/cns/stninfo.pl?stn=112 August 2004.

Panday, S., and P. S. Huyakorn (2004), A fully coupled physically-based spatially-distributed model for evaluating surface/subsurface flow, *Advances in Water Resources*, *27*, 361-382.

Perotto, S. (2006), Adaptive modeling for free-surface flows, *ESAIM: Mathematical Modelling and Numerical Analysis*, *40(3)*, 469-499.

Qian, J. (2006), Approximations for viscosity solutions of Hamilton-Jacobi equations with locally varying time and space grids, *SIAM Journal for Numerical Analysis*, *43(6)*, 2371-2401.

S. S. Papadopulos Associates, Inc. (2007), Groundwater flow model for administration and management in the Lower Rio Grande basin (Draft).

Tang, H., and G. Warnecke (2006), High resolution schemes for conservation laws and convection-diffusion equations with varying time and space grids, *Journal of Computational Mathematics*, *24(2)*, 121-140.

U. S. Geological Survey (2008), The National Map Viewer Website, http://nmviewogc.cr.usgs.gov/viewer.htm June 2008.

Weeden, A. and T. Maddock III (1999), Simulation of Groundwater Flow in the Rincon Valley Area and Mesilla Basin, New Mexico and Texas, University of Arizona Research Laboratory for Riparian Studies and Department of Hydrology and Water Resources.

Zhang, X. D., J. Y. Trépanier, M. Reggio, and R. Camarero (1994), Time-accurate local time stepping method based on flux updating, *AIAA Journal*, *32(9)*, 1926-1929.

Distribution

1	MS0123	LDRD Office	1011 (electronic copy)
1	MS0899	Technical Library	9536 (electronic copy)
1	~~MS1350~~MS0735	Vince Tidwell	6313 (electronic copy)

All electronic copies below:

MS0123	Yolanda Moreno	1012
MS0706	Peter Kobos	6312
MS0735	Ray Finley	6313
MS0735	Thomas Lowry	6313
MS0735	John Merson	6310
MS0735	Suzanne Pierce	6313
MS0735	Marissa Reno	6313
MS0735	Amy Sun	6313
MS0751	James Brainard	6311
~~MS0887~~	~~Duane Dimos~~	~~1800~~
MS1108	Mike Hightower	6332
~~MS1138~~	~~Steve Conrad~~	~~6322~~
MS1350	Geoff Klise	6313
MS1350	Len Malczynski	6313
MS1350	Howard Passell	6313
MS1350	Will Peplinski	6313
MS1350	Elizabeth Richards	6313
MS1350	Jesse Roach	6313

Suzanne Tillery (New Mexico State University)
James Phillip King (New Mexico State University)


Sandia National Laboratories